UNIVERSITY OF OKLAHOMA

GRADUATE COLLEGE

PRACTICAL EXTENSIONS TO THE EVALUATION AND ANALYSIS OF WIRELESS COEXISTENCE IN UNLICENSED BANDS

A DISSERTATION

SUBMITTED TO THE GRADUATE FACULTY

in partial fulfillment of the requirements for the

Degree of

DOCTOR OF PHILOSOPHY

By

MOHAMAD OMAR AL KALAA
Norman, Oklahoma
2016

PRACTICAL EXTENSIONS TO THE EVALUATION AND ANALYSIS OF WIRELESS COEXISTENCE IN UNLICENSED BANDS

A DISSERTATION APPROVED FOR THE
SCHOOL OF ELECTRICAL AND COMPUTER ENGINEERING

BY

Dr. Hazem H. Refai, Chair

Dr. Timothy Ford

Dr. Ali Imran

Dr. Thordur Runolfsson

Dr. Kam Wai Clifford Chan

To my father, mother, sister, brothers, and my wife.

Acknowledgements

I would like to thank Dr. Hazem Refai for his continuous support, encouragement, and friendship.

The participation of Dr. Ford, Dr. Imran, Dr. Runolfsson, and Dr. Chan in my doctoral committee, and their support is greatly appreciated.

My sincere gratitude goes to my wife, Rawan, who's unbound faith in me and unconditional support were the pillars I stood upon during my journey.

My parents, Ghassan and Amal; sister, Leila; brothers, Amer, Tawfiq, Issam, and Kais, are all acknowledged for their love and support every step of the way.

Michelle Farabough is acknowledged for her effort in editing this dissertation.

My heartfelt recognition goes to the OU-Tulsa family of students, alumni, and staff.

Contents

List of Tables

List of Figures

Abstract

Sharing spectrum resources in unlicensed bands has proven cost effective and beneficial for providing ubiquitous access to wireless functionality for a broad range of applications. Chipsets designed to implement communication standards in the Industrial, Scientific and Medical (ISM) band have become increasingly inexpensive and widely available, making wireless-enabled medical and non-medical devices attractive to an increased number of users. Consequently, wireless coexistence becomes a concern. In response, the U.S. Food and Drug Administration (FDA) has issued a guidance document to assist medical device manufacturers ensure reasonable safety and effectiveness. Coexistence-testing methods are now being reported in literature, and novel solutions are under consideration for inclusion in the American National Standards Institute (ANSI) C63.27 Standard for Evaluation of Wireless Coexistence.

This dissertation addresses practical issues for evaluating and reporting wireless coexistence. During testing, an under-test-system (UTS) is evaluated in the presence of an interfering system (IS). Accordingly, an innovative method is suggested for estimating channel utilization of multiple, concurrent wireless transmitters sharing an unlicensed band in the context of radiated open environment coexistence testing (ROECT). Passively received power measurements were collected, and then a Gaus-

sian mixture model (GMM) was used to build a classifier for labeling observed power samples relative to their source. Overall accuracy was verified at 98.86%. Case studies are presented utilizing IEEE 802.11n as an IS with UTS based on either IEEE 802.11n or ZigBee. Results demonstrated the mutual effect of spectrum sharing on both IS and UTS in terms of per-second channel utilization and frame collision.

The process of approximating the probability of a device to coexist in its intended environment is discussed, and a generalized framework for modeling the environment is presented. An 84-day spectrum survey of the 2.4 GHz to 2.48 GHz ISM band in a hospital environment serves as proof of concept. A custom platform was used to monitor power flux spectral density and record received power in both an intensive care unit (ICU) and a post-surgery recovery room (RR). Observations indicated that significant correlation in activity patterns corresponded mainly to IEEE 802.11 channels 1, 6, and 11. Consequently, channel utilization of three non-overlapping channels of 20 MHz bandwidth—relative to IEEE 802.11 channels 1, 6, and 11—were calculated and fitted to a generalized extreme value (GEV) distribution. Low channel utilization ($<$10%), along with sporadic occurrences of higher channel utilization ($>$50%), was observed in the surveyed environment. Reported findings can be complementary to wireless coexistence testing.

Quantifying the probability of UTS coexistence in a given environment is central to the evaluation of coexistence, as evidenced in the draft of the C63.27 standard. Notably, a method for this calculation is not currently provided in the standard. To fill this void, the work presented herein proposes the use of logistic regression (LR) to estimate coexistence probability. ROECT was utilized to test a scenario with an

802.11n IS and ZigBee UTS medical device. Findings demonstrate that fitted LR model achieves 92.72% overall accuracy of classification on a testing dataset that included the outcome of a wide variety of coexistence testing scenarios. Results were incorporated with those reported in [1] using Monte Carlo simulation to estimate UTS probability of coexistence in a hospital environment.

Chapter 1: Introduction

1.1. Motivation

Wireless technology plays an instrumental role in modern life. Licensed and shared-spectrum usage paradigms have been implemented for multiple applications. The former serves as the basis of application-specific usage, such as cellular communication, television broadcast, and medical implants communication systems (MICS). The latter has experienced an exponential growth in popularity due to the availability, maturity, and low cost of technologies that operate in unlicensed bands (e.g., 2.4 GHz Industrial, Scientific, and Medical [ISM] band). Economic and logistic forces, as well as the race for innovation, have motivated medical device manufacturers to equip their products with wireless interfaces running technologies like Wi-Fi, ZigBee, and Bluetooth. In 2013, the wireless portable medical device market was valued at $7.52 billion; this figure is expected to grow to $17.71 billion in 2020 [2]. The contention for unlicensed spectrum resources raises concerns about wireless coexistence, especially regarding sensitive applications like those used in medical devices. Currently, there are no standardized methods for wireless coexistence testing. Instead, many assessments are ad hoc.

Joint work to develop a standardized method to assess wireless coexistence—

primarily for medical devices—is currently underway by Subcommittee 7 of American National Standards Institute (ANSI)-accredited standards committee (ASC) C63® (designated C63.27, Standard for Evaluation of Wireless Coexistence [3]) and the Wireless Working Group (SM-WG06) of the Association for the Advancement of Medical Instrumentation (AAMI) TIR 69/Ed. 1 [4]. The ANSI subcommittee details coexistence testing methodology and reporting for medical and non-medical devices. The AAMI group addresses risk assessment of integrating a wireless technology in a medical function.

In the following section, practical aspects of wireless coexistence testing are presented to address necessary questions like what to test, how to test, and how to present the results.

1.2. Coexistence testing methods

1.2.1 What to test?

During testing, the wireless functionality of an under-test-system (UTS) is evaluated relative to interference caused by an interfering system (IS) (i.e., a system that shares the spectrum with the UTS). Typically, UTS/IS comprises transmitter (Tx) and receiver (Rx) nodes. Coexistence depends on adequate spectrum resource sharing in terms of time, frequency, and power. Successful performance of UTS wireless functionality requires a given minimum period (i.e., time) of channel access (i.e., time-on-air or channel utilization [CU]) while maintaining a signal-to-interference-plus-noise (SINR) ratio higher than a minimum to facilitate proper demodulation.

Accordingly, an elevated IS CU could deprive UTS from channel access and result in failure of UTS wireless functionality. Testing will aid in identifying the IS CU threshold at which IS and UTS can coexist. This can be accomplished by configuring IS to operate on maximum throughput (i.e., maximum IS CU). If UTS fails, IS throughput is decreased and the test is repeated until IS CU threshold allows coexistence.

Similarly, separation distance between UTS/IS could be increased upon UTS failure to identify minimum distance necessary for successful UTS wireless operation. Alternatively, IS transmission power (i.e., interference level in SINR) could be varied to establish the ratio of UTS/IS signal levels for successful UTS wireless functionality. Notably, received power level at a node's antenna is inversely proportional to separation distance from the transmitting node. When UTS operates on a static channel (e.g., Wi-Fi or ZigBee), testing is performed where IS occupies a co/adjacent channels relative to UTS. However, when UTS employs a frequency hopping scheme (e.g., Bluetooth), IS could be set to operate on one or more channels that overlap UTS usage. Wi-Fi has been identified in the literature as the system generating the most severe interference in the 2.4 GHz ISM band [1,5]. Consequently, for basic evaluation, IS could be set to operate on Wi-Fi channel 6 (i.e., blocking one third of the 2.4 GHz ISM band and leaving two thirds for Bluetooth use). A more rigorous level of evaluation could be achieved by setting IS to simultaneously operate on Wi-Fi channels 1, 6, and 11 [6] (i.e., three interfering networks in band blocking configuration). Either a signal generator or an actual network implementation could be used to emulate IS. However, due to lack of channel sensing ability, results could differ when an IS is based on a signal generator as opposed to utilizing an actual network [7].

1.2.2 How to test?

Several coexistence-testing methods have been proposed in the literature, many of which are being considered in ANSI C63.27. In [8], Young et al. reviewed a number of methods and discussed corresponding coexistence factors. Testing methodologies are generally based on the medium used to establish a communication channel between IS and UTS nodes; these are divided into conducted and radiated methods.

Conducted testing

For conducted testing, communication between IS and UTS nodes is established through a wired system using coaxial cables, couplers/splitters, and attenuators (See Figure 1.1, where arrows represent coaxial cables). Monitoring equipment is introduced to the channel to facilitate detection and identification of coexistence variables limits. Attenuators are used to emulate path loss experienced by propagating wireless signals in realistic environments. Manzi et al. used conducted testing to evaluate coexistence of ultra-wide band (UWB) radios and Wi-Fi [9]. A major challenge with this method is that it requires physical access to all antennae ports on the IS and UTS nodes, which could be impossible when antennae are embedded. Also, path loss estimation is required to emulate a given intended UTS deployment environment.

Radiated testing

Radiated testing alleviates the need of direct access to a node's antenna port by replacing the conducted communication path with over-the-air propagation. Following

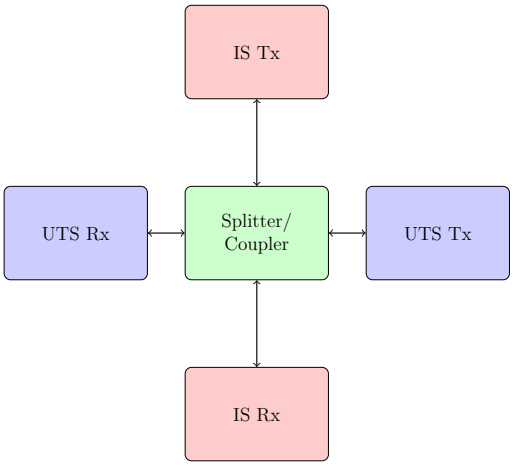

Figure 1.1. Conducted testing layout

are two variations of radiated testing.

- *Two Anechoic Chambers:* In this scenario, each UTS node is placed in an anechoic chamber equipped with an antenna to capture the node's propagating signals that are fed through a coaxial cable. Afterwards, signals from IS nodes are introduced to the communication path through a splitter/coupler that connects nodes and the anechoic chambers. Figure 1.2 illustrates this setup; arrows represent coaxial cables. In [10], Remley et al. used a radiated two-anechoic chamber setup to verify wireless device performance for equipment used by emergency responders. Similar to the conducted test setup, path loss is assumed to be known. Free-space path loss inside each chamber and external attenuators are utilized to emulate realistic path loss. Notably, this setup adds the burden of having access to two anechoic chambers, which could be costly and requires the service of commercial testing labs. Another burden is the calibration of anechoic chambers prior to each test.

- *Open environment:* In this scenario, UTS and IS nodes are deployed in an ac-

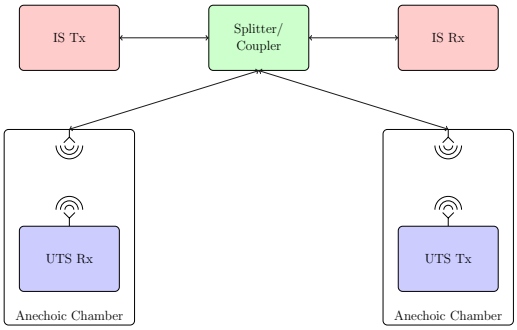

Figure 1.2. Radiated using two anechoic chambers testing layout

tual indoor environment (e.g., room) to allow realistic signal propagation to occur not unlike actual UTS deployment in its intended environment. Consequently, path loss is not calibrated. Instead, separation distance between nodes is controlled either directly or by configuring nodes' transmission power. Exposed and hidden terminal scenarios are tested using a variation of line-of-sight (LOS) and non-line-of-sight (NLOS) setups. Ambient signals and the environment noise floor are monitored to ensure testing is not influenced by unintended signals. This setup is depicted in Figure 1.3. Radiated open environment setup was used by LaSorte et al. in [11] to test ZigBee-based medical devices for wireless coexistence with 802.11g interferer. Given the lack of controlled communication path, testing outcome based on this setup exhibits larger variance, as noted in [8]. Appendix A of this work addresses quantifying the repeatability and reproducibility of radiated open environment coexistence testing. Integrating monitoring equipment in this setup is challenging. A solution is therefore proposed in Chapter 2. An alternative to the open environment could be an anechoic chamber that eliminates wave reflection and multipath. This approach was suggested for coexistence testing in [6].

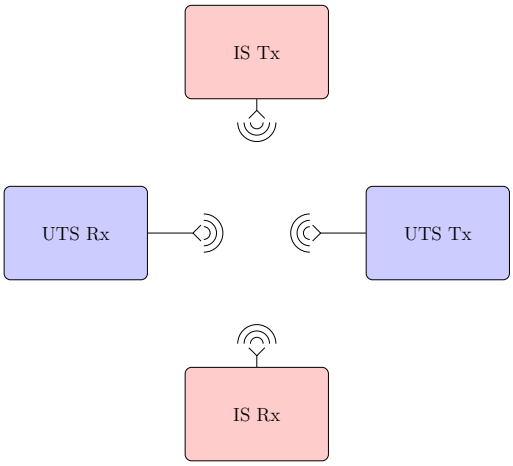

Figure 1.3. Radiated open environment testing layout

1.2.3 How to present the results?

Coexistence testing results are organized in a report that includes UTS technical specifications (e.g., wireless technology, sensitivity, system architecture) and IS technical specifications (e.g., hardware implementation, firmware version, transmission power), as well as testing setup. UTS pass/fail criteria should be clearly defined and justified according to the definition of UTS wireless functionality. Furthermore, coexistence testing should address the mutual effect of UTS and IS. This can be accomplished by reporting throughput/CU—or another performance metric—of UTS and IS as a time series that spans the testing period. This way, inhibitive effects of UTS on coexisting networks could be detected, given that they exist. Chapter 2 details CU classification and reporting for multiple coexisting systems in a radiated open environment setup.

One useful method to present testing results is through coexistence probability. Logistic regression could be leveraged to establish a formula of binary test outcome (i.e., pass or fail) as a function of testing variables (e.g., IS throughput, IS transmission power). Given that testing outcome had more than two states, multinomial

logistic regression could be used. Chapter 4 presents a detailed case-study in which logistic regression is employed to summarize coexistence testing results. A complementary step is incorporating spectrum survey measurements from UTS intended environment. Spectrum surveys could be performed following International Telecommunication Union (ITU) recommendations [12]. Accordingly, a long-term spectrum survey of a hospital environment was performed and presented in [1, 13]. The outcome of this type of spectrum measurement campaign is a statistical distribution of observed CU values in the investigated environment. Subsequently, simulation (i.e., where environment CU distribution and UTS coexistence testing regression model serve as inputs) could provide insight about expected probability of UTS coexistence when deployed in an intended environment.

1.3. Contribution

Contributions of this dissertation include the following.

1. Development of a method to monitor ROECT based on Gaussian mixture model classifier. This method is in response to the need for a monitoring algorithm for ROECT, given lack of accessible communication path when compared to radiated two-anechoic chambers and conducted testing methodologies. The suggested method is implemented and validated using experimental data. The method accurately estimates the CU of multiple coexisting wireless systems based on passive power measurements collected in time-domain using a generic vector signal analyzer.

2. Establishment of a foundation for finding a robust statistical model of the electromagnetic environment in which a medical device would typically operate. A long-term spectrum survey was conducted, and a parallel program for data processing was developed. Daily CU of monitored sub-channels was first investigated to gain insight about present wireless technologies in the environment. Consequently, per-second CU of Wi-Fi channels 1, 6, and 11 was calculated and fitted to generalized extreme value distribution. This work is utilized to help advance standardization of coexistence evaluation for medical devices.

3. Framework conception for calculating the probability of coexistence. Given the lack of clear methodology in current standardization efforts to perform such calculation, logistic regression is suggested as a statistical tool for associating the outcome of coexistence testing with a number of testing variables. Suggested method is evaluated through experimental data. Furthermore, simulation is employed to assess the probability of coexistence in an intended environment by using the outcome of a spectrum survey. Results are presented in such a way as to assist industry, regulators, and testing laboratories prepare coexistence testing reports.

The balance of this dissertation is organized as follows. Chapter 2 introduces a method to monitor ROECT setup through post-processing of over-the-air power measurements collected in time domain. Gaussian mixture model classifier is trained and used to identify CU of each participating system. An implementation and validation study of the classifier is discussed wherein IS was 802.11n [14] and UTS was first

802.11n and then ZigBee [15]. Findings prove useful for inclusion in a typical coexistence testing report. Chapter 3 elaborates on a long-term spectrum survey of the 2.4 GHz ISM band in a hospital environment. The measurement system, as well as the methodology, is detailed. Results include a statistical distribution of CU values observed during survey period. In Chapter 4, logistic regression is proposed in a framework to estimate coexistence probability. A demonstration of the framework is conducted through testing wherein IS was 802.11n and UTS was ZigBee. Afterwards, Monte Carlo simulation was performed—based on the results of work detailed in Chapter 3—to estimate UTS coexistence probability in its intended environment. Related work is provided in each chapter with respect to the discussion at hand. Chapter 5 concludes the dissertation. Finally, Appendix A presents a study of the repeatability and reproducibility of ROECT.

Chapter 2: Monitoring ROECT using GMM classifier

2.1. Introduction

Healthcare applications are an essential part of the emerging Internet of Things (IoT), which promises to advance the human way of life to a new smart era [16]. Wireless technology lies at the foundation of the IoT and is a ubiquitous facilitator of communication for health related applications, as well as others [17]. The abundance of low-cost hardware for implementing wireless protocols in unlicensed bands (e.g., the 2.4 GHz industrial, scientific, and medical [ISM] band) has been the impetus for increased attention from manufacturers. Accordingly, technologies such as Wi-Fi, Bluetooth, and ZigBee, to name a few, have been successfully introduced to support medical device wireless functionality. The result is a rising concern about wireless coexistence. The U. S. Food and Drug Administration (FDA) has acknowledged this issue and recommended that medical device manufacturers address wireless coexistence in their protocol before gaining clearance to introduce products into the market. The FDA guidance defines wireless coexistence as *the ability of one wireless system to perform a task in a given shared environment where other systems (in that environment) have an ability to perform their tasks and might or might not be using the same set of rules* [18]. Medical device manufacturers wishing to participate in the

IoT era are integrating wireless communication in their products. Consequently, they need to comply with the FDA guidance for wireless coexistence.

Subcommittee 7 of the American National Standards Institute (ANSI)-accredited standards committee (ASC) C63® has responded to the need for a standard to regulate wireless coexistence testing by initiating work on C63.27 American National Standard for Evaluation of Wireless Coexistence, currently in drafting stage. Contributors to the standard include academicians, industry representatives, and scientists from universities and federal agencies, including the FDA and the National Institute of Standards and Technology (NIST). Suggested testing methods include the use of RF cables, combiners, splitters, and signal generators to create a wired link between communicating nodes of the under-test-system (UTS) and interfering system (IS) node(s). However, this method requires access to antenna ports on all nodes participating in the test, which might be impractical or even impossible in scenarios where device antenna ports are inaccessible. Radiated methods have since been introduced to overcome this issue. These can now be performed either by placing participating nodes in one [6] or several [10] anechoic chambers, or by using a low-noise environment [11]. The latter is labeled radiated open environment coexistence testing (ROECT). Details and comparison of coexistence testing methods is provided by Young et al. in [8]. Methods other than ROECT allow direct access to the signal path of both UTS and IS, thus making the tasks of monitoring the test and reporting channel utilization (CU) of systems relatively easy.

This work proposes a classifier based on Gaussian mixture model (GMM) for categorizing observed power values during the ROECT process. In addition, an algorithm

to estimate CU of each active device in ROECT is detailed. Identifying CU of two interfering systems illustrates the mutual effect of their coexistence in the shared, all-connected environment of the IoT. Using an IEEE 802.11n network as interferer, two case studies are discussed below wherein UTS operates on either 802.11n or ZigBee in terms of per-second channel utilization and frame collisions.

The balance of this chapter is organized as follows. Section 2.2 provides a summary of research regarding the use of GMM for characterization of wireless networks. GMM formulation, ROECT, and the proposed method are introduced in Section 2.3. Section 2.4 details experimental work for classifier validation and expands on case studies wherein the system under test is either 802.11n or ZigBee. Finally, Section 2.5 concludes the chapter.

2.2. Related work

GMM has been used for a wide range of wireless network applications. Authors in [19] observed that in a typical indoor scenario for Ultra-Wide Band (UWB) impulse radio systems, interference is the result of multiple interferers that may or may not have different power levels. The work demonstrates that GMM is a natural modeling choice to jointly capture interference characteristics.

Detection of 802.11 medium access control (MAC) layer spoofing was reported successful in [20] by modeling received signal strength (RSS) using GMM. The authors exploited antenna diversity of 802.11 transmitters and obtained a profile of legitimate signal sources. Spoofing packets were identified by testing the hypothesis that newly observed RSS values fit the model. Gulati et al. [21] proposed a GMM-based algorithm

to identify intruders in a network through wireless channel characterization as opposed to investigating RSS values. Channel fingerprints from a legitimate user and from an intruder were estimated to belong to separate GMM components. This allows classifying arriving packets into legitimate and intruding classes. Another example of enhancing communication security using GMM was reported in [22]. Authors relied on the timing of persons' heartbeats—modeled by four-component GMM—to secure communication in wireless body area network (WBAN) as a replacement for a key exchange authentication paradigm.

RSS values have been repeatedly used for positioning and localization purposes. In [23], GMM was used to determine cellular base station positions and to identify spatial spectrum holes for cognitive radio purposes. The inherent problem is localizing multiple unknown radio sources using a mobile measurement station. To enhance localization accuracy in indoor environments, GMM can be used to detect and exclude RSS outlier measurements [24]. Two-mode GMM is employed to model both normal patterns and outliers. Based on prior knowledge of Wi-Fi access point (AP) deployment locations, GMM was used in [25] to model RSS of multiple APs and then determine the location of an indoor mobile unit.

By having the flexibility to model several sub-populations of observations within one large data set, GMM usage can be extended to activity classification based on accelerometer readings. For example, authors in [26] attempted to monitor and identify patient activities in a home environment. To do so, they modeled accelerometer data gathered by on-body sensors and transmitted wirelessly using ZigBee by leveraging GMM to classify continuously executed morning activities (e.g., brushing, washing,

and shaving). A training dataset was constructed from data representative of performing each activity, and then testing data of continuous activities were classified. The suggested model achieved 88.3% classification accuracy. Similarly, classification of athletic activities using several forms of classifiers is presented in [27]. In [28], wearable sensors were used to collect ECG, heart sound, respiration, and SPO2 signals during sleep. This data was sent via Bluetooth to a personal computer. Signals were modeled using GMM to detect obstructive sleep apnea patterns.

Other uses include modeling packet error rate in vehicular ad-hoc networks (VANET) as a function of distance [29], speaker [30], and language [31] recognition, as well as improving iris recognition by detecting eyelid and eyelashes in an image [32].

Mutual interference of coexisting wireless technologies in unlicensed bands using radiated testing have been heavily investigated in literature. For example, homogeneous, simultaneously active 802.11b/g/n networks were evaluated in [5]. Effects of 802.11g on ZigBee during the course of coexistence testing were presented in [11]. Interference between co-located ZigBee nodes was analyzed in [33]. CU of industrial wireless sensor networks (WSNs) following multiple spectrum sharing techniques was investigated in [34]. Notably, CU of separate nodes participating in testing were never reported. The novelty in the method proposed in this dissertation is that it is the first to use probabilistic modeling, particularly GMM, to provide insight about CU during ROECT. This work adds essential information about the effect of an interfering system on UTS, as well as the reverse case (i.e., the effect of UTS on surrounding networks) and the footprint of its communication in time.

2.3. Methodology

2.3.1 Gaussian Mixture Model

GMM was used to build a power measurement classifier based on data obtained during ROECT. GMM was selected based on its ability to represent multiple clusters of observations in a data set. Each cluster includes power value measurements generated by wireless activity of a unique ROECT transmitter. GMM density function is defined as a linear combination of K Gaussian components

$$p(x|\theta) = \sum_{k=1}^{K} \pi_k \mathcal{N}(x|\mu_k, \sigma_k^2) \tag{2.1}$$

where $\mathcal{N}(x|\mu_k, \sigma_k^2) = \frac{1}{\sigma\sqrt{2\pi}} \exp -\frac{1}{2}\left(\frac{x-\mu_k}{\sigma_k}\right)^2$ is a Gaussian normal distribution with mean μ_k and standard deviation σ_k; π_k are mixing weights that satisfy $0 \leq \pi_k \leq 1$; and $\sum_{k=1}^{K} \pi_k = 1$. GMM parameters π_k, μ_k, and σ_k can be estimated using the expectation maximization (EM) algorithm first presented in [35]. EM is an iterative algorithm that assumes prior knowledge of K and commences with an initial guess of model parameters. Data sample classification is based on a given $p(x|\theta)$ and determined by finding component k with the largest posterior probability for observation i.

$$r_{i,k} = \frac{\pi_k \mathcal{N}\left(x_i|\mu_k, \sigma_k^2\right)}{\sum_{k'=1}^{K} \pi_{k'} \mathcal{N}\left(x_i|\mu_{k'}, \sigma_{k'}^2\right)} \tag{2.2}$$

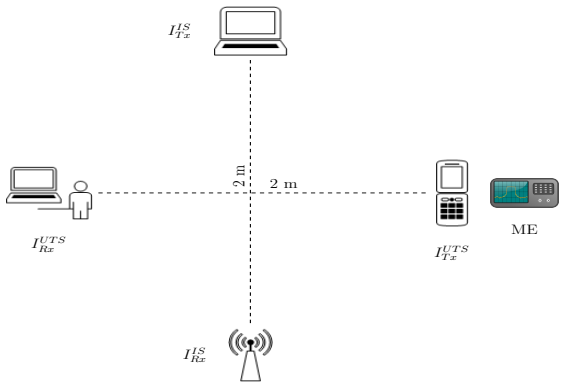

Figure 2.1. ROECT test layout.

2.3.2 Channel utilization

A typical ROECT line-of-sight (LOS) test layout is depicted in Figure 2.1. The following three systems are used in ROECT.

Interfering system (IS)

IS comprises a transmitter node (I_{Tx}^{IS}) and a receiver node (I_{Rx}^{IS}). Using actual wireless networks, as opposed to signal generators, is suggested as a source of interference in the C63.27 standard draft. For example, Wi-Fi networks are typically used as an interferer when testing wireless medical devices [6]. Notably, Wi-Fi transmissions that are performed strictly by sending a stream of packets on the wireless link from I_{Tx}^{IS} to I_{Rx}^{IS} will incur transmission of acknowledgment (ACK) packets on the reverse link. Data, ACK, and management frames contribute to CU originating from IS.

System under test (UTS)

UTS comprises a transmitter node (I_{Tx}^{UTS}) and a receiver node (I_{Rx}^{UTS}). Investigated wireless functionality could include half- or full-duplex transmission. Therefore, it is

best to identify CU resulting from each UTS node.

Monitoring equipment (ME)

ME provides passive measurements of ongoing wireless channel activity (e.g., spectrum analyzer, vector signal analyzer, or software defined radio [SDR], among others).

Received power at ME antenna, P_r, is a function of the separation distance between wireless signal source and its transmission power. Therefore, when both IS and UTS are active during an observation window, an empirical probability density function (PDF) of P_r values will show multiple peaks, representing samples from the following signals: noise, IS Tx, IS Rx, UTS Tx, and UTS Rx. Consequently, a mixture probabilistic model of observed P_r values permits proper representation of sub-populations in the sample set of power measurements. In fact, a GMM can be constructed to approximate any given density [36]. CU is defined as the fraction of time during which a wireless channel is busy. Consequently, for CU generated by activities of system x, CU_x is the ratio of observed power samples generated by x while active relative to total number of samples during an integration time (IT). Hereafter in this chapter, IT = 1 s [12].

2.3.3 ROECT characterization

Figure 2.2 illustrates that ME observed activity of a given source (i.e., transmission of a packet) can be divided into three regions: 1) rising edge R_r, 2) active transmission R_a, and 3) falling edge R_f. Compared with R_a where power samples fluctuate around a mean, both R_r and R_f exhibit a distinct range of values. Consequently,

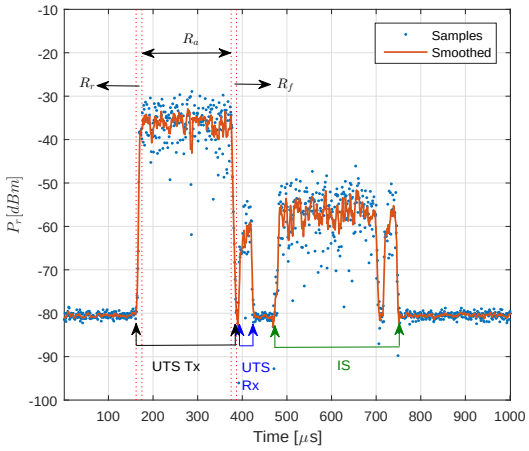

Figure 2.2. Power measurements observed at ME.

if EM algorithm is used to estimate the parameters of GMM components modeling noise and device x activity, samples from R_r and R_f will contribute to increasing the variance of the component modeling the latter. Consequently, overlap between adjacent GMM components increases and classification accuracy decreases. Hence, k-means clustering algorithm was used in this work to estimate the centroid of the clusters. Variance of GMM components was set to a fixed value.

The following 5-step procedure is proposed for identifying CU of IS and UTS nodes during coexistence testing. For step i, a representative data set of power measurements, S_i, is collected using ME.

Step 1 Characterize noise samples while IS and UTS are off

Samples of S_1 are fitted to a Gaussian distribution to estimate the mean μ_N and variance σ_N^2 of noise samples.

Step 2 Characterize interferer while UTS is off

IS is set to operate at a fixed power level regardless of modulation or data rate. This facilitates the identification of CU_{UTS} in case UTS uses adaptive power levels. K-means clustering algorithm [37] is used to find the centroids of three clusters: noise μ_N; IS Tx μ_{Tx}^{IS}; and IS Rx μ_{Rx}^{IS}. The former is ignored due to the fact that it was accurately estimated (i.e., without the presence of other sample populations) in the previous step. In the event that ME was symmetrically located with respect to I_{Tx}^{IS} and I_{Rx}^{IS}, two clusters would be sufficient.

Step 3 Characterize UTS while IS is off

μ_{Tx}^{UTS} and μ_{Rx}^{UTS} are estimated similar to Step 2. Given that UTS uses multiple transmission power levels, more than three clusters must be identified. To do so, the appropriate number of clusters can be found by running k-means iteratively with an increasing number of clusters k, and then selecting k value at which the lowest Akaike information criterion (AIC) is observed.

Step 4 Build GMM classifier

Step 4 requires the use of equation 2.1 with μ_N, σ_N^2, μ_{Tx}^{IS}, μ_{Rx}^{IS}, μ_{Tx}^{UTS}, and μ_{Rx}^{UTS} to construct a GMM. Since no prior information is available for mixing weights in a test data set, a uniform assumption was placed on π_k. Missing variance values are set to a fixed constant ν.

Step 5 Classification of test data

Using the obtained model, test data are classified into GMM component yielding the highest posterior probability. While this process is adequate for R_a samples, the result is classifying samples from R_r and R_f to components closer to their range of values rather than the component matching samples identified for R_a. To correct the misclassification, label correction procedure (LCP) is needed. Labels of noise bound samples (i.e., in-between two occurrences of noise samples) are modified according to the label of their majority. In concept, this is similar to detecting outliers using the Hampel filter, which replaces data samples in a window that are distant from the median with the median value.

LCP guarantees that samples from regions R_r and R_f are correctly classified following R_a class. Furthermore, LCP corrects outliers in R_a, as shown in Figure 2.3. Frame collision occurs when device x transmits while device y is active, which might corrupt frame reception at the receiver due to decreased signal-to-noise-plus-interference ratio (SINR). The short separation distance between ME and one of the active transmitters results in saturation of the ME RF front-end. Therefore, when a collision occurs, power samples are classified as originating solely from the nearby transmitter. Consequently, observed noise bound samples will belong to multiple classes. LCP facilitates the detection of frame collision by 1) finding the majority label in noise bound samples; 2) allowing continuous occurrences (of length η) for samples labeled differently from the majority to retain their GMM assigned label; and 3) changing the balance of the samples to the majority label.

2.3.4 Limitations

Two limitations to the proposed method were identified. The first is inherited from monitoring time-domain measurements that are focused on a narrow bandwidth. Consequently, frequency hopping systems such as Bluetooth will require the use of monitoring equipment with wide instantaneous bandwidth and a high sampling rate. For example, Bluetooth hops randomly on 79 channels, each with 1 MHz bandwidth for a duration of 625 μs. To capture such activity, ME must maintain a sampling rate faster than the hopping rate when monitoring the entire 80 MHz band used by Bluetooth.

Second, the closer the means of adjacent GMM components, the less accurate the classification decision. Consider the case of two adjacent Gaussians $\mathcal{N}(\mu_1, \sigma^2)$ and $\mathcal{N}(\mu_2, \sigma^2)$ where $\mu_1 < \mu_2$. The threshold, γ_1, at which $e\%$ of $\mathcal{N}(\mu_1, \sigma^2)$ density is determined can be calculated as

$$\gamma_1 = \mu_1 + \sigma Q^{-1}(e) \tag{2.3}$$

where $Q^{-1}(\bullet)$ is the inverse Q function $Q(x) = \frac{1}{\sqrt{2\pi}} \int_x^\infty \exp\left(\frac{-t^2}{2}\right) dt$. Similarly, γ_2, at which $e\%$ of $\mathcal{N}(\mu_2, \sigma^2)$ density is

$$\gamma_2 = \mu_2 - \sigma Q^{-1}(e) \tag{2.4}$$

The distance between μ_1 and μ_2 resulting in $e\%$ error for $\mathcal{N}(\mu_1, \sigma^2)$ and $\mathcal{N}(\mu_2, \sigma^2)$

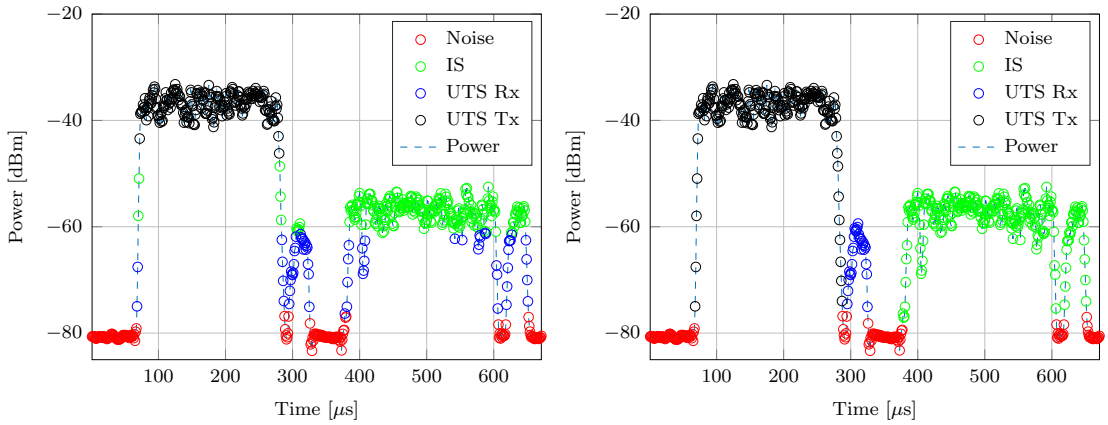

(a) Before LCP **(b)** After applying LCP

Figure 2.3. An example of labeled power samples before and after LCP. It can be noted that LCP successfully assigns the correct label to contiguous transmissions.

can then be found as:

$$\mu_2 - \mu_1 = 2\sigma Q^{-1}(e) \tag{2.5}$$

Noise bound samples are classified following the label of their majority. Therefore, $e\% < 50\%$ can be tolerated, which guarantees that the majority of samples are correctly classified. However, extremely short transmissions are prone to misclassification due to the limited number of observed samples. This error can be accounted for by increasing ME sampling rate. Distance between adjacent components can be adjusted (i.e., values of μ_1 and μ_2 can be shifted) by changing the deployment location of the ME or adjusting transmission power of wireless nodes, if appropriate.

2.4. Experimental work

Power measurements in dBm are collected in time domain with an I/Q sampling rate of 1×10^6 sample/s. Center frequency is set to match the desired channel used for

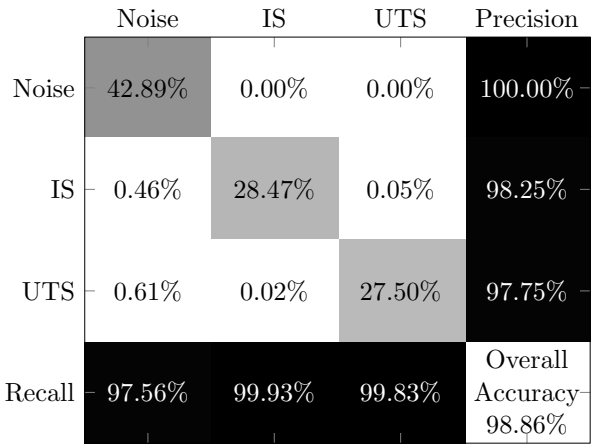

Figure 2.4. Classifier confusion matrix.

communication. Time-domain measurements capture only a narrow bandwidth at a high rate, as opposed to frequency-domain measurements where a frequency sweep is performed. Channel activity by wireless protocols such as 802.11 and ZigBee is on the scale of microsecond (e. g., short inter-frame space (SIFS) for 802.11n is 10 μs). Therefore, time-domain measurements allow data acquisition at a rate fast enough to capture changes in active/inactive status of the channel. Monitoring a narrow-band of an active transmitter's channel is assumed representative of transmitter activity on the entire channel it occupies. For example, an 802.11n transmitter simultaneously occupies 20 MHz bandwidth when active; thus, observing a part of that band is indicative of the activity of the entire band. The hardware used in this work to collect power measurements was manufactured by National Instruments (NI) and included PXIe-1082 chassis populated with PXIe-8133 controller, PXIe-5644R vector signal transceiver (VST), and 2 dBi omnidirectional antenna. LabView data collection software developed at the University of Oklahoma (OU) [38] is used for I/Q sample acquisition, power level calculation, and storage. Testing layout is illustrated in Figure

2.1. ME is placed at 15 cm behind I_{Tx}^{UTS} in a symmetric position relative to I_{Tx}^{IS} and I_{Rx}^{IS}. Consequently, P_r generated by IS is observed with equal levels at ME. When processing P_r data for an active transmitter (i.e., in R_a), values were observed fluctuating in a wide range primarily due to multipath propagation and intrinsic changes in power levels during frame transmission when using a given modulation scheme. To limit the effect of these variations on the estimation algorithm and to exploit the used low-value variance in GMM classifier, a smoothing filter of length $L = 5$ samples was implemented during a preprocessing stage. Exemplary raw and smoothed power values are plotted in Figure 2.2.

Tests were performed for a 60 s period. Based on empirical observations, variance of GMM components representing UTS and IS were set to $\nu = 1$. Low variance permitted lower overlap between adjacent components and directed the classifier to focus on accurately labeling samples that were closer to the mean of a given component. As addressed in Section 2.3.4, LCP corrected misclassification due to component overlap—of which inaccurate variance value is a contributing factor. To detect collision, a consecutive non-majority-compliant samples window was set to $\eta = 25\ \mu s$. CU is presented for IT = 1 s. The dataset collected during 60 s was divided into 60 equal parts, and each was processed individually.

2.4.1 Validation

Both IS and UTS were set to operate on 802.11n. Data sets of 1 s observation period (i.e., $\approx 1 \times 10^6$ samples) were obtained to train the classifier, as described in Section 2.3.3. Mean value of received power measurements for noise, IS, UTS Tx, and UTS Rx

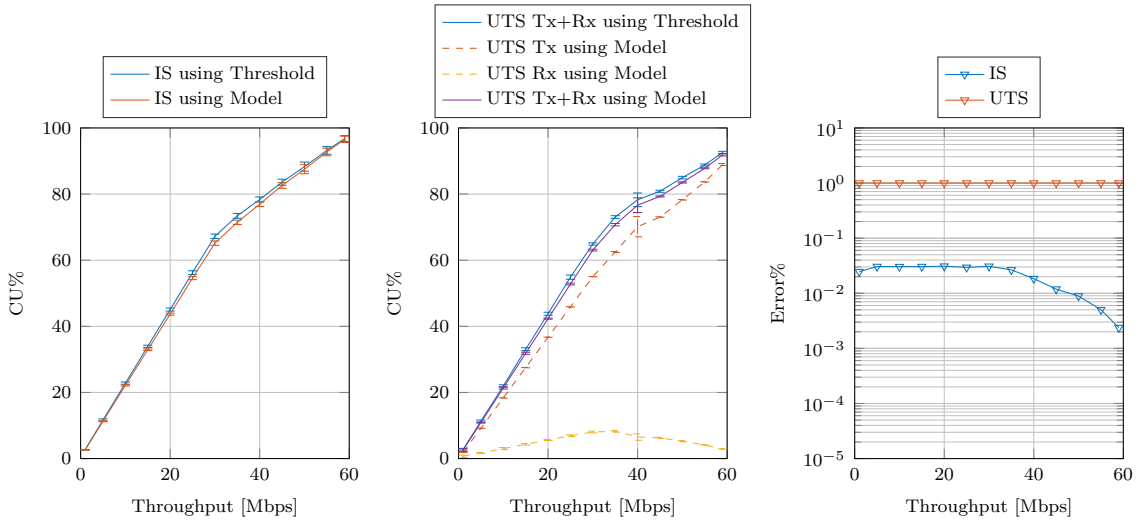

(a) IS CU

(b) UTS CU

(c) Error between GMM estimated and threshold estimated CU

Figure 2.5. Validation of classifier using data observed by varying the throughput of IS and UTS systems and comparing with a naive thresholding approach.

were estimated to -80.7 dBm, -58.55 dBm, -36.79 dBm, and -63.75 dBm, respectively. While UTS was powered off, IS was set to operate at a fixed throughput for 60 s, and ME was used to collect P_r measurements. Consequently, 60 samples of CU were obtained for each test run. Throughput value was increased each test-run until the maximum was reached for a total of 13 test-runs. Data traffic was UDP with message size of 1500 bytes. The same process was repeated for UTS while IS was powered off. A validation data set was constructed by joining samples of all 26 test-runs. A naive approach based on direct thresholding was used to obtain true labels for samples from each test run. Threshold was calculated as three standard deviations higher than the noise mean, or 99% confidence, for detecting accurate channel activity. Since only one system was enabled during any given test run, all samples above the threshold were labeled according to the operational system. Samples below the threshold were

labeled as noise. Three classes were verified using this approach, namely noise, IS, and UTS. Samples originating from I_{Tx}^{UTS} and I_{Rx}^{UTS} were grouped into a single class since thresholding is only able to identify samples above the noise threshold (i.e., binary decision). Classifier performance is detailed in Figure 2.4 where the confusion matrix is illustrated. Overall accuracy was 98.86%.

The comparison between classifier estimated CU^{GMM} and threshold-based CU, CU^{T}, is plotted in Figure 2.5. An error bar represents the mean and standard deviation of the corresponding CU for every data point on Figure 2.5(a) and Figure 2.5(b). Error is calculated as

$$Error = \frac{\left| E\left[CU^{T}\right] - E\left[CU^{GMM}\right] \right|}{E\left[CU^{T}\right]} \tag{2.6}$$

where $E[\bullet]$ denotes the mean CU value in a given test-run. Notably, classifier estimates CU within a maximum error of 1%. 802.11n introduced several improvements over older 802.11 standards (e.g., 802.11b/g), including frame aggregation and block acknowledgments. The behavior of both is captured in Figure 2.5(b). For high throughput values, UTS Rx (i.e., ACK packets) consume less CU when compared to low throughput values, the reason being that multiple MAC Service Data Units (MSDU) are aggregated at UTS Tx into one frame that is acknowledged by UTS Rx using a single block ACK message. This explains the piece-wise linear relationship between CU and throughput for 802.11n, as opposed to the linear relationship exhibited by 802.11b/g and reported in [5].

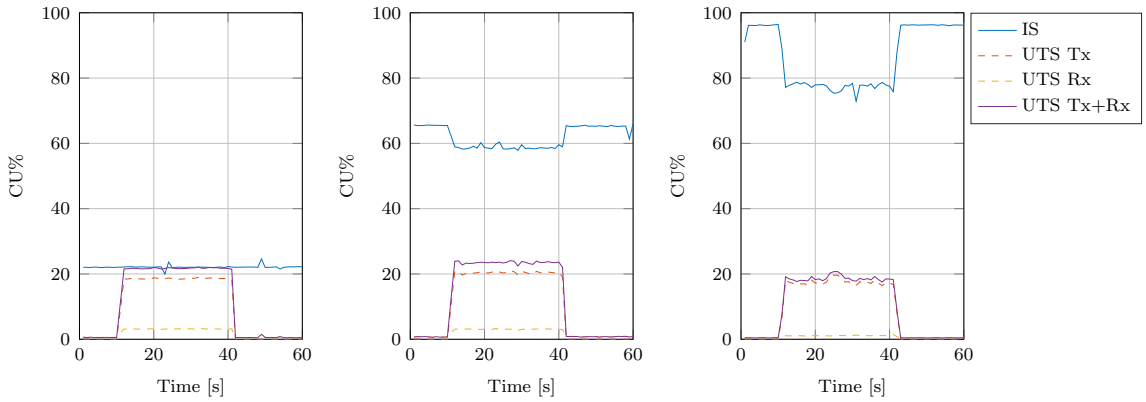

(a) Low, 10 Mbps **(b)** Medium, 30 Mbps **(c)** High, 60 Mbps

Figure 2.6. Example of ROECT where both IS and UTS use 802.11n.

2.4.2 UTS Case Studies

IEEE 802.11n

UTS[1] used IEEE 802.11n to initiate communication at a throughput of 10 Mbps for 30 s. This case is representative of a medical device basestation uploading an activity log to a central server through an access point. IS represents an IEEE 802.11n network operating at one of the following throughput values: 60 Mbps, 30 Mbps, or 10 Mbps, representing high, medium, and low interference levels, respectively. Results of these three experiments are depicted in Figure 2.6. When interference was low (Figure 2.6(a)), UTS was able to coexist successfully with IS and share the channel without noticeable reduction in either system CU. Consequently, both systems retained communication at the desired throughput. When interference was medium (Figure 2.6(b)) and UTS joined the channel, IS had to share the channel, which resulted in reduced CU. Relatively, IS communication throughput was slightly decreased to 27

[1]Both access point and station for UTS and IS were realized using Mikrotik RouterBOARD RB953GS equipped with R11e-2HPnD radio card.

Mbps. In this case, UTS succeeded in fulfilling its wireless function. Figure 2.6(c) demonstrates a case of high interference. Both IS and UTS exhibited decreased performance when UTS joined the channel. In this case, IS was operating at maximum achievable throughput $\approx$ 60 Mbps with CU$\approx$ 96%. When UTS was enabled, contention between the two systems—both using CSMA/CA for medium access control (MAC)—forced IS to refrain from channel access while UTS was transmitting. Due to contention for channel resources and frame collisions, IS throughput decreased to 42 Mbps and UTS achieved an average throughput of 9 Mbps. The decrease in throughput conforms with results reported in [5].

Frame collisions detected by LCP for the same three scenarios are plotted in Figure 2.7. Each data point corresponds to the count of collisions in IT = 1 s observed when IS operated at a given throughput. Collisions observed during medium interference were higher than those observed during high interference, primarily because under medium throughput, there are longer inactivity periods between transmissions. Therefore, UTS has a greater chance of gaining channel access and suffering from frame collision as opposed to a case of high throughput where a UTS is deprived from channel access because of very short inactivity periods. Examples of frame collisions are illustrated in Figure 2.9(a) and Figure 2.9(b) and show that a transmission was incurred by either IS or UTS when the channel was preoccupied by the other system's activity.

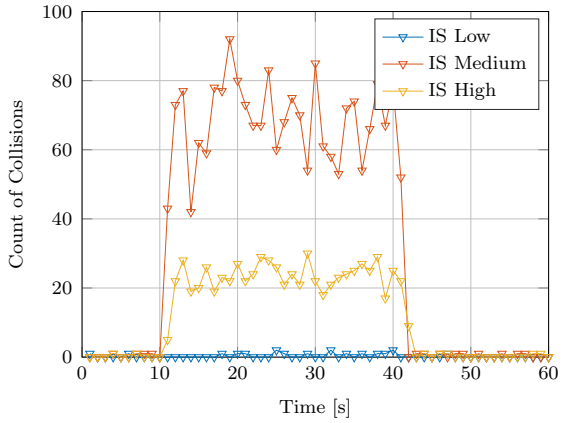

Figure 2.7. Frame collisions when both UTS and IS use 802.11n.

ZigBee

IEEE 802.15.4-based nodes, to which ZigBee subscribes, are a popular low-power, low-cost choice for several applications in the IoT realm [39]. For example, a healthcare application detailed in [40] used 802.15.4 transceivers as a part of smart monitoring and tracking system in healthcare facilities. ZigBee node I_{Tx}^{UTS} served as a UTS, transmitting two packets per second and receiving data at companion node, I_{Rx}^{UTS}[2]. The investigated transmission period was 60 s with a total of 120 packets. ZigBee packet loss was tracked as IS throughput increased for each test-run until the maximum was reached. UTS Tx performed clear channel assessment (CCA) prior to each packet transmission. Results of the case study are illustrated in Figure 2.8. Figure 2.8(a) plots ZigBee packet loss rate as a function of IS throughput, and Figure 2.8(b) plots mean CU as a function of IS throughput. Figure 2.8(c) depicts the count of detected frame collisions. Figure 2.8(a) illustrates that ZigBee packet loss increases as IS throughput increases. Total packet loss was observed near the high end of

[2]Both using Texas Instruments (TI) CC2530 development boards.

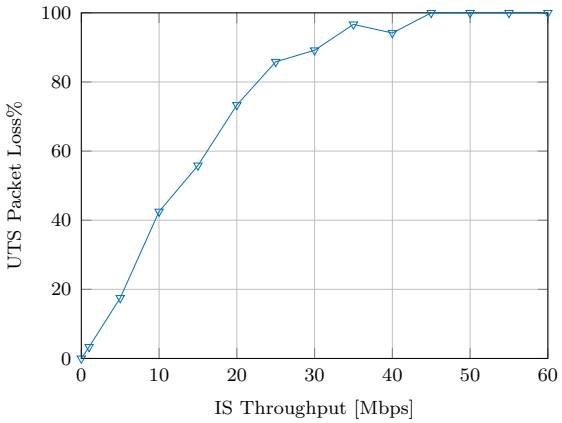

(a) Packet Loss

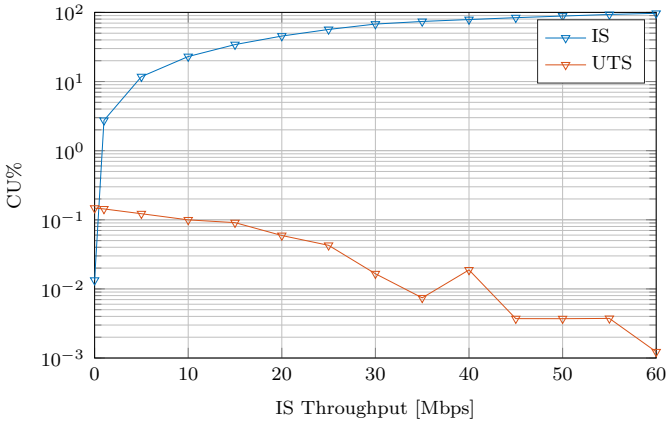

(b) CU

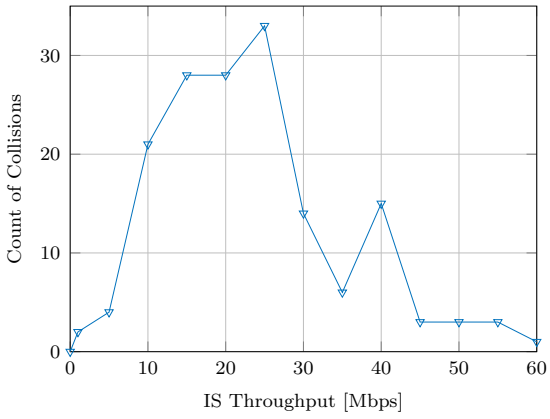

(c) Collisions

Figure 2.8. Example of ROECT where IS uses 802.11n and UTS uses ZigBee.

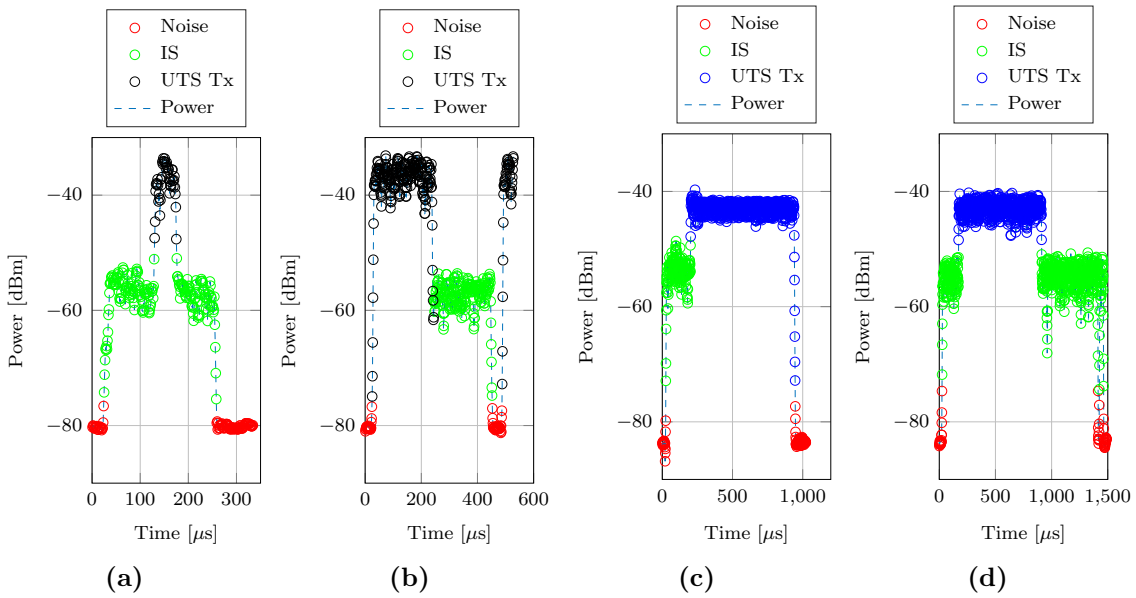

Figure 2.9. Frame collisions detected by LCP. A collision occurs when either IS or UTS begins transmission while the channel is busy with the other system's activity. (a), (b) UTS is 802.11n. (c), (d) UTS is ZigBee.

throughput values. Similar to the observation reported above for the case 802.11n UTS, when IS throughput was near the high end of values, the CCA timer of ZigBee UTS was forced to expire as a result of the high CU of IS. This is illustrated in Figure 2.8(b). Consequently, ZigBee packet was dropped, which follows the case of an exposed terminal. However, when IS throughput was in the medium range of values, UTS Tx was able to successfully perform CCA and transmit. Notably, collision can occur (e.g., Figure 2.8(c)), corrupting packet reception at the UTS Rx due to low SINR. Examples of frame collisions are illustrated in Figure 2.9(c) and Figure 2.9(d).

2.5. Conclusion

A GMM-based classifier was introduced for use in ROECT monitoring. The classifier was able to label passive power measurements obtained with monitoring equipment based on their source. By doing so, channel utilization during coexistence testing was quantified for both IS and UTS. Achieved overall accuracy was 98.86%. Two case-studies were introduced to observe how collocated systems interact while sharing spectrum resources. Findings of observed performance for 802.11n and ZigBee systems conform with those reported in literature.

Chapter 3: Spectrum survey in hospital environments

3.1. Introduction

Medical device manufacturers are integrating Wi-Fi and Bluetooth technology into medical devices to spur innovation in healthcare. These wireless technologies use the 2.4 GHz industrial, scientific, and medical (ISM) unlicensed band, and share spectrum with other wireless devices, consequently increasing the likelihood of communication loss and errors. Unlike spectrum bands that are dedicated for medical use (e.g., wireless medical telemetry service [WMTS][1] and medical implant communications service [MICS][2]), the ISM band was intended for a broad range of applications (e.g., industrial or domestic) that generate and use radio frequency energy [41]. The unlicensed nature of the ISM band, coupled with the maturity of technologies it accommodates, such as Wi-Fi and Bluetooth, have made it a popular choice for an increasing number of wireless-enabled medical devices. For example, [6] reports that the majority of wireless medical devices cleared by the U.S. Food and Drug Administration (FDA) utilize either Bluetooth or Wi-Fi. One challenge of incorporating wireless communication into a medical device is ensuring reasonable safety and effectiveness [42]. Consequently, the FDA issued a guidance document regarding the use of wireless

[1] 608-614 MHz, 1395-1400 MHz, and 1427-1432 MHz
[2] 401-406 MHz, 413-419 MHz, 426-432 MHz, 438-444 MHz, and 451-457 MHz

radio-frequency (RF) technology [18]. Recommendations suggest that medical device manufacturers address wireless coexistence in their premarket submission (i.e., application for permission to market the device). The FDA guidance defines wireless coexistence as *the ability of one wireless system to perform a task in a given shared environment where other systems (in that environment) have an ability to perform their tasks and might or might not be using the same set of rules.* Notably, there are currently no standardized test methods for such an assessment. Consequently, many wireless coexistence tests are performed ad hoc.

3.1.1 Coexistence: Standardization and Methods

Work toward developing a standardized process for RF wireless coexistence assessment is currently underway by Subcommittee 7 (Spectrum Etiquette) of American National Standards Institute (ANSI))-accredited standards committee (ASC) C63®. ANSI is a private, non-profit organization that oversees the development of voluntary consensus standards in the United States. ANSI also coordinates U.S. standards with international standards. The future standard, currently in draft, is designated C63.27, Standard for Evaluation of Wireless Coexistence [3]. After a wireless device is tested for coexistence, an optional next step is to derive the approximate probability of the device coexistence ability in its intended environment. The work detailed in this dissertation provides the foundation for approximating this probability by providing a generalized framework to model the intended environment of the device under test. Experimental data is provided to show the application of this framework.

Several methods have been suggested in literature and are under review for inclu-

sion in C63.27 [8]. One uses RF components (e.g., combiners, couplers, and attenuators) to establish a wired communication link between medical device wireless nodes so that interference can be introduced through the use of signal generators or by way of an actual wireless network. This form of testing is referred to as *conducted testing* and has the downside of requiring access to the medical device's antenna ports. *Radiated testing* does not require access to device antenna ports and can be performed in an anechoic chamber [6], two smaller anechoic chambers [10, 43], or in alternative low-noise environments [11]. Similar radiated methods of characterization are known as over-the-air (OTA) testing in several domains, such as the cellular network research [44]. Recently, the use of reverberation chambers has been suggested [45] to introduce electromagnetic fields that emulate interference in realistic environments.

Although suggested coexistence testing methods differ, the goal is to characterize medical devices in terms of the basic physical layer coexistence parameters of distance, frequency, and time, as well as how the higher Open Systems Interconnection (OSI) layers mitigate interference. Notably, the physical layer of a receiving node could experience blocking—which cannot be mitigated in higher OSI layers—due to transmitters in close proximity on the same or adjacent RF channels. Furthermore, when operating in close range of other transmitters, electromagnetic coupling could affect the performance of a medical device (e.g., [46]). Such effects are addressed by testing for electromagnetic compatibility (EMC) and electromagnetic immunity (EMI) following standards like International Electrotechnical Committee (IEC) standard IEC 60601-1-2:2014 [47]. However, coexistence evaluation primarily focuses on the performance of a medical device while under interference from other wireless transmitters

sharing the spectrum.

When experiencing interference, a medical device's Signal to Interference Plus Noise Ratio (SINR) decreases. This can be emulated by controlling distance—physically or by varying transmission power/attenuation—to provide insight about expected medical device performance relative to its separation distance from an interfering network. The interferer's operating frequency can be set on a channel that overlaps the one used by the medical device (i.e., co-channel) or on an adjacent channel that could cause interference as a result of imperfect filtering. The result would be a decrease in SINR. Both scenarios can be accounted for during testing by controlling the interfering node's RF parameters. The probability of successful packet transmission increases when channel occupancy time (i.e., channel utilization-(CU) or duty cycle) decreases. The CU threshold at which a medical device can successfully achieve its wireless functions can be determined by varying the interferer's throughput.

3.1.2 Contribution

The main contribution in this chapter is establishing a foundation for finding a robust statistical model of the electromagnetic environment in which a medical device would typically operate. Such statistics are reported in a way that could be meaningful to the healthcare community. Coexistence testing protocols address devices under test utilizing a broad range of standardized or proprietary wireless protocols. CU of monitored sub-channels can be averaged over 24-h and reported as a function of frequency to provide insight about frequently occupied and frequently available sub-channels. With regard to sources of interference, the Wi-Fi family of protocols operating on

20 MHz bandwidths can generate elevated CU of 80%-90% [5]. Therefore, these protocols pose the most serious interference threat for devices in their vicinity sharing the spectrum [48]. As such, and based on the observations of 24-h CU average of individual sub-channels, CU of Wi-Fi[3] channels 1, 6, and 11 was measured and fitted to a generalized extreme value distribution. CU quantifies wireless spectrum occupancy, which is associated with the likelihood that new devices attempting to use the spectrum will experience during wireless coexistence. Results are presented to highlight the temporal distribution of CU relative to the time of day. An example of expected coexistence behavior of a wireless device in the surveyed environment is discussed in Section 3.4.2, given the relationship between the allowed time window of the device's wireless functions and measured CU.

The remainder of this chapter is organized as follows. Section 3.2 presents background information about previous spectrum surveys and methods used for evaluation. Section 3.3 describes the location, experimental setup, and methodology for spectrum survey measurements. Section 3.4 presents experimental results that can be used by the healthcare community. Finally, Section 3.5 concludes the chapter.

3.2. Related work

Spectrum surveys have attracted the interest of a wide variety of groups, including government agencies [49, 50], corporations [51], and academicians [52]. The National Telecommunications and Information Administration (NTIA) of the United States Department of Commerce conducted several outdoor broadband spectrum surveys in

[3]Wi-Fi and IEEE 802.11 are used interchangeably.

the late 1990s. Surveyed locations included Denver, CO and San Diego, Los Angeles, and San Francisco, CA. Some surveys have recently been repeated (e.g., San Diego and Denver), and new ones have been conducted in Chicago, IL [50]. Activities in the 2.4 GHz ISM band were identified as unique to the measurement locations and attributed to background RF radiation generated by ISM devices and microwave ovens.

Microsoft Spectrum Observatory [51] was launched in response to the NTIA Spectrum Monitoring Pilot Program Notice of Inquiry [53]. Bands between 30 MHz and 6 GHz are monitored at locations distributed worldwide using Ettus Universal Software Radio Peripherals (USRPs) devices. Collected data are centrally stored and processed for visualization through the Windows Azure Cloud and are made freely available to the public. Main output parameters include observed power density, utilization, and spectrograms, all of which can be obtained dynamically online. In July 2007, the Illinois Institute of Technology (IIT) started a permanent spectrum monitoring system in Chicago. The system is able to interface with various data collection hardware. Some use a scan-based approach, offering wider observation bandwidth at the expense of lower time resolution. Others use higher sampling rate focusing on narrow bands (i.e., time-domain electromagnetic interference approach [54]), thus generating high time resolution measurements. The project has expanded to incorporate multinational collaborators, including Virginia Tech (VT), Blacksburg, VA, USA; Turku University of Applied Sciences (TUAS), Turku, Finland; University of Oulu, Oulu, Finland; and VTT Technical Research Centre, Finland [52]. Storage and data analysis aspects of the project are reported in [55].

Authors in [56] present results of a spectrum survey of the 2.3-2.4 GHz band conducted at locations in Europe and the United States wherein the band was scanned for three seconds. The survey was executed for two non-contiguous weeks during two consecutive months. Average and maximum powers of daily recorded measurements were reported. When calculating occupancy, decision threshold was set to -93 dBm to observe extremely low frequency band occupancy (FBO) $< 1\%$. Integrated power and occupancy—both measured instantaneously and also with a 5-minute moving average filter—were reported as time series given in days. Similar reports, including spectrograms, were used for data from Chicago. Previously, authors employed a Fluke Networks PC Card Sensor attached to a laptop for obtaining power and CU measurements in the ISM band [57]. Measurement bandwidth of 156 kHz was used to generate 641 frequency bins. Testing locations were a university library and a residential area in Finland.

Outside the scope of the IIT consortium, considerable worldwide effort has been invested in spectrum surveys. Eight locations, including residential, commercial, and university campus sites, were surveyed in Oulu, Finland and reported in [58]. Each survey investigated the 2.4 GHz ISM band for one week. Authors intended to introduce a new cognitive radio (CR) system to operate in the ISM band and to propose a method entitled Transmission Encapsulation based on the Connected Component Labeling (TECCL). TECCL identifies continuously occupied frequency blocks (e.g., wide-band transmissions) by substituting low power measurements within each block. A Fluke Networks PC Card Sensor was utilized to collect data. This sensor provides CU measurements with a decision threshold of 20 dB above the noise floor and an

integration time of one second. Frequency bin bandwidth was 156 KHz, generating 641 bins and completely covering the 2.4 GHz ISM band. A comparative analysis was performed using Agilent N6841A RF sensor, generating 916 frequency bins with a sweep time of 10 mS. TMote Sky sensor nodes were deployed in [59] to monitor the 16 IEEE 802.15.4 channels and to provide a collective reading of the 2.4 GHz ISM band for identifying spectrum opportunities. Authors reported average CU in time and frequency and also provided a table specifying peak usage observations for each location.

A long term, wideband spectrum survey in Singapore is reported in [60]. The study lasted 12 days and covered spectrum bands between 80 MHz and 5850 MHz. Authors used LabView controlled Agilent E4407B spectrum analyzer to collect measurements. Reported parameters include maximum power as a function of frequency; spectrogram with applied threshold (i.e., binary color depth); and CU as a function of frequency. Authors could not detect occupancy in the 2.4 GHz ISM band. Results were attributed to the large distance that separated the deployed measurement device and any 2.4 GHz ISM network.

A collaborative study between the University of Bristol, United Kingdom and Toshiba Research Europe Ltd. is presented in [61]. Bands between 300 MHz and 4.9 GHz were monitored in Bristol for six months. Authors attempted to describe occupancy observations throughout various days and times for use in cognitive radio applications. The measurement system was based on a PC controlled spectrum analyzer equipped with two antennas. Bandwidth resolution was 20 kHz. In addition to illustrating CU readings on the surveyed band, authors reported mean occupancy

across the entire band to highlight periodic variations of activity.

In [62], authors in Eindhoven, Netherlands, focused on the 2.36-2.4 GHz band allocated for medical body area networks (MBAN). The measurement system was based on Rohde & Schwarz ZVL6 spectrum analyzer, which was controlled by a laptop. Spectrograms covering 24 hours of measurements were presented, as well as maximum/minimum/average-recorded power. Complementary Cumulative Distribution Function (CCDF) of the received power was examined and plotted for multiple frequencies. Cumulative Distribution Function (CDF) of active/idle time for multiple center frequencies were presented, as well.

Miguel López-Benítez has extensively researched spectrum occupancy for cognitive radio applications. His research is detailed in many conference and journal publications and is included in his PhD thesis [63]. López-Benítez relied heavily on empirical spectrum measurements for his studies. The author established methodological aspects of spectrum occupancy evaluation in the context of cognitive radio [64]. In [65], López-Benítez presented results of a spectrum measurement campaign performed over a rich range of practical scenarios in a densely populated, indoor and outdoor urban environment located in the city of Barcelona, Spain. The measurement system was based on an Anritsu Spectrum Master MS2721B spectrum analyzer. Results were presented as CU with 24-hour integration time. Low CU ($< 10\%$) was observed for the 2.4 GHz ISM band at surveyed locations. In [66], time domain spectrum occupancy (i.e., CU as a function of time of day), was grounded on a two-state, discrete-time Markov chain. The model was based on empirical measurements conducted over seven days on each investigated band. Duty cycle models pertaining to

cellular mobile communication systems were developed based on deterministic and stochastic approaches. In the former, CU evolution with time was modeled as the sum of multiple bell-shaped exponential terms. In the latter, CU values were drawn from either Beta or Kumaraswamy distributions.

Several researchers performed spectrum surveys in hospitals in the 1970s, including McDonnell Douglas Astronautics Co.-East under contract to the FDA Bureau of Medical Devices[4]. McDonnell Douglas used the survey data to draft a medical device EMC standard [49], which includes citations of spectrum measurements made by other researchers. In 2003 researchers used a spectrum analyzer to survey several locations at two hospitals in Virginia over several days including the intensive care unit (ICU) and radiography units [67]. High disturbance levels were rarely reported. Characteristics of wireless channels (i.e., path loss and power delay profile [PDP]) in several bands used in medical applications were also surveyed in a hospital room in Japan [68]. In 2009, hospital surveys in Switzerland [69] and Oklahoma, USA [70] were reported. The Swiss survey found evidence of rare electric field levels exceeding the 3 V/m immunity test level specified by IEC standard 60601-1-2 [47] for non-life supporting medical equipment; the Oklahoma survey did not find these same results. In addition to Wi-Fi and Bluetooth signals, microwave oven radiation was observed at Kyoto University Hospital in 2013, as detailed in [71]. More recently, multiple surveys of hospitals in Finland [72–74] and Italy [75] were reported in literature. Researchers adopted similar observation methods by deploying a spectrum analyzer at various locations in investigated hospitals. Received RF power was recorded and

[4]Under FDA contract 223-74-5246

used to report CU. Findings were analogous and included low spectrum occupancy observations. A short-term survey of an ICU conducted using a vector signal analyzer was employed to evaluate Bluetooth Low Energy (BLE) for wireless coexistence in [76].

To the best of this author's knowledge, literature has yet to report spectrum surveys of hospital environments extending over a period of time similar to the study detailed in this chapter. The integration between data collection equipment and a supercomputer processing platform enabled efficient and flexible analysis of the large volume of data collected over nearly three months. Results reported in this chapter are published in [13] and [1].

3.3. Setup & Methodology

The surveyed locations for the work detailed in this chapter are located at the University of Oklahoma (OU) Medical Center campus in downtown Oklahoma City, OK, USA. The combined facilities comprise the largest hospital in the state of Oklahoma. A vector signal analyzer (VSA) was used for measurement hardware. The VSA has an average noise level of –157 dBm/Hz, 80 dB spurious-free dynamic range (SFDR), and 50 MHz instantaneous bandwidth (at 3 dB). Test equipment were installed in a networking-equipment cabinet in a 24/7 operational post-surgery recovery room (RR) and in an ICU, where the equipment was connected to a nearby 9 dBi omnidirectional antenna using a low-loss cable fed through a dropped ceiling. Signal loss caused by cable length and antenna gain are accounted for in data collection software. The RR was equipped with 16 hospital beds, each separated by a curtain. The antenna

was placed at the RR entrance. The ICU accommodates 13 beds, each located in a separate room. In this scenario, the antenna was placed in the hallway connecting the ICU rooms. With hospital staff assistance, the survey lasted for 84 days, commencing December 4, 2014, and ending February 25, 2015.

Data collection software developed at OU [38] was used to collect dBm power measurements by scanning the wireless spectrum between 2.4 GHz and 2.48 GHz. Without averaging, instantaneous power measurements were acquired on a total of 1993 frequency bins, each having 40 kHz bandwidth during a total dwell time of 4 ms for hardware installed at RR and 6 ms in the ICU. Random processing and disc I/O time increased the average spectrum sweep capture time to approximately 12 ms at RR and 16 ms at ICU. Measured dBm power samples were logged in text files, wherein each line represented one spectrum sweep. To facilitate data storage, a daily directory was created, and power samples in one-minute intervals were grouped into a single subdirectory. Approximately 11.8 TB of data was collected and stored at the Tandy Supercomputing Center in Tulsa, OK, where a parallel program was developed for fast data processing.

A threshold is required for making a decision as to whether a channel is active or inactive at any given time. Methods for selecting an appropriate decision threshold T have been investigated extensively and reported in literature. One such method suggests simply selecting T by visual inspection of power measurements, and then deciding on a level that separates activity patterns from noise [74]. Further automation of the threshold selection process can be completed by inspecting noise measurements to find the mean and maximum recorded noise values. Afterwards, T can be consid-

ered to equal the maximum noise value, thus minimizing false detection that would occur if noise samples were identified as genuine activity. Alternatively, T can be calculated as several dB above the mean noise value. For example, the International Telecommunication Union (ITU) spectrum occupancy measurements and subsequent evaluation report suggest that the threshold should be at least 3 dB to 5 dB above the noise level [12]. In this method, noise variance contributes to false detection of noise samples as activity. A compromise between "maximum noise value" and "mean plus several dB" methods was adopted for this study by selecting a given probability of false detections and calculating the value of T accordingly. Several measurement windows of 1-min duration were examined empirically. A high-activity window was then selected to derive a probability distribution function (PDF) of power values. Because noise samples are considered normally distributed, the threshold was fixed at two standard deviations from the noise mean, which is equivalent to 95% confidence in accurate activity detection. The assumption was that the noise threshold was constant throughout the survey period. Consequently, the decision threshold was fixed at $T = -79.84$ dBm for RR and $T = -81.88$ dBm for ICU.

CU is the fraction of time a given channel is detected as active by way of observing power values exceeding the decision threshold. This method conforms with the ITU definition of frequency band occupancy (FBO) [12]. In Section 3.4.2, CU values were calculated using 1 s time resolution mapping variations in spectrum occupancy throughout the day. To do so, each minute of collected data was divided into 60 equal parts, assuming that power measurements were taken at a constant rate over a 1-min period. After applying threshold T to power measurements of a given Wi-Fi channel

C collected at time instance n, a binary matrix $\mathcal{X}_C^{s\times b}(n)$ was constructed, where s (i.e., number of rows) is the count of spectrum sweeps collected during 1 s; $b = 500$ (i.e., number of columns) is the number of 40 kHz sub-channels in 20 MHz; and $x_{i,j}$ is the binary result of comparing the corresponding power measurement with T, yielding "0" given measured power is $< T$ and otherwise yielding "1." Consequently, CU for time instance n is:

$$\Phi_C(n) = \frac{1}{sb}\sum_{i=1}^{s}\sum_{j=1}^{b} x_{i,j} \tag{3.1}$$

When $b = 1$ and s equals the count of spectrum sweeps during 24 h, $\Phi_c(n)$ refers to the CU of a given 40 kHz sub-channel c over 24 h integration time. For clarity, we denote this case as $\phi(f_i)$, where f_i is a given 40 kHz sub-channel, as detailed in Section 3.4.1.

CU quantifies the percentage of time the channel is occupied, which is a fundamental parameter for investigating and testing for coexistence [6, 7, 11]. It should be noted that measurements in this work, and others as reported in literature, were performed at one location per survey. Wireless traffic sources contributing to calculated CU values are those near the data collection antenna. The unlicensed character of the 2.4 GHz ISM band and the spectrum management practices of hospital staff, as well as human or machine demand to offered wireless services, are all factors supporting the uniqueness of each spectrum survey.

3.4. Results

CU of monitored sub-channels is averaged over 24 h and reported as a function of frequency for both RR and ICU locations. Afterwards, CU was used as a measure of spectrum occupancy in Wi-Fi channels 1, 6, and 11 with 20 MHz bandwidth centered on 2412 MHz, 2437 MHz, and 2462 MHz, respectively, at RR. These three channels were found most active in this particular environment [13]. Other wireless systems that operate in the 2.4 GHz ISM band include Bluetooth and ZigBee. Bluetooth uses an adaptive frequency hopping (AFH) mechanism to avoid interference on any of its 79 channels of 1 MHz bandwidth or 37 channels of 2 MHz bandwidth in the event that BLE is used. ZigBee uses 16 non-overlapping channels of 2 MHz bandwidth and typically uses much lower transmission power compared to Wi-Fi. Consequently, both systems have minimal contribution to the reported CU values. However, acquiring spectrum measurements at a frequency resolution higher than the bandwidth of Wi-Fi, Bluetooth, or ZigBee (40 kHz in comparison with 20 MHz, 1 MHz, and 2 MHz, respectively) allows capture of such activities when they occur in the vicinity of the monitoring antenna within a given spectrum sweep.

3.4.1 CU evaluation using 24 h integration time

In this section, spectrum measurements are presented for RR and ICU locations during 28 days. $\phi(f_i)$ where $f_i \in [2.4, 2.48]\ GHz$ covering $M = 1993$ sub-channels at RR and ICU locations are presented in Figures 3.1 and 3.2, respectively. Weekdays are illustrated on separate sub-figures, each containing four curves to account for the

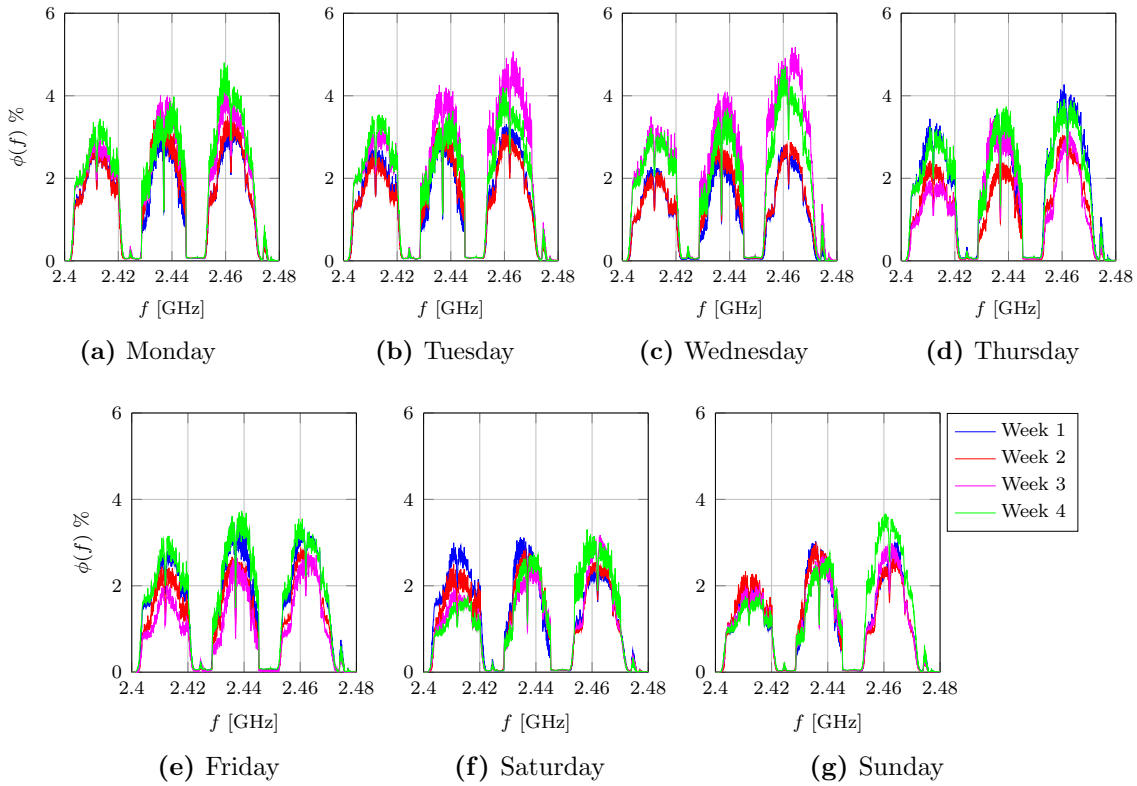

(a) Monday **(b)** Tuesday **(c)** Wednesday **(d)** Thursday

(e) Friday **(f)** Saturday **(g)** Sunday

Figure 3.1. $\phi(f_i)$ **at RR**

28 day (i.e., four week) survey subset. Occupancy patterns matching IEEE 802.11 activities on channels 1, 6, and 11 (i.e., 20 MHz bandwidth centered on 2.412, 2.437, and 2.462 MHz, respectively) can be observed for RR in Figure 3.1.

Figure 3.2 demonstrates that spectrum occupancy differs between ICU and RR locations. Occupancy subscribing to IEEE 802.11 pattern is observed mainly on frequencies belonging to channels 6 and 11, indicating that nearby access points primarily employed these two channels to provide WiFi access. Moreover, the recurrent presence of narrow-band activities of approximately 2 MHz bandwidth centered on $f_k = 2402 + k \times 2\ [MHz], k = 0, ..., 39$ were found to behave similar to BLE activity pattern. Another difference in observations between the two locations can be made

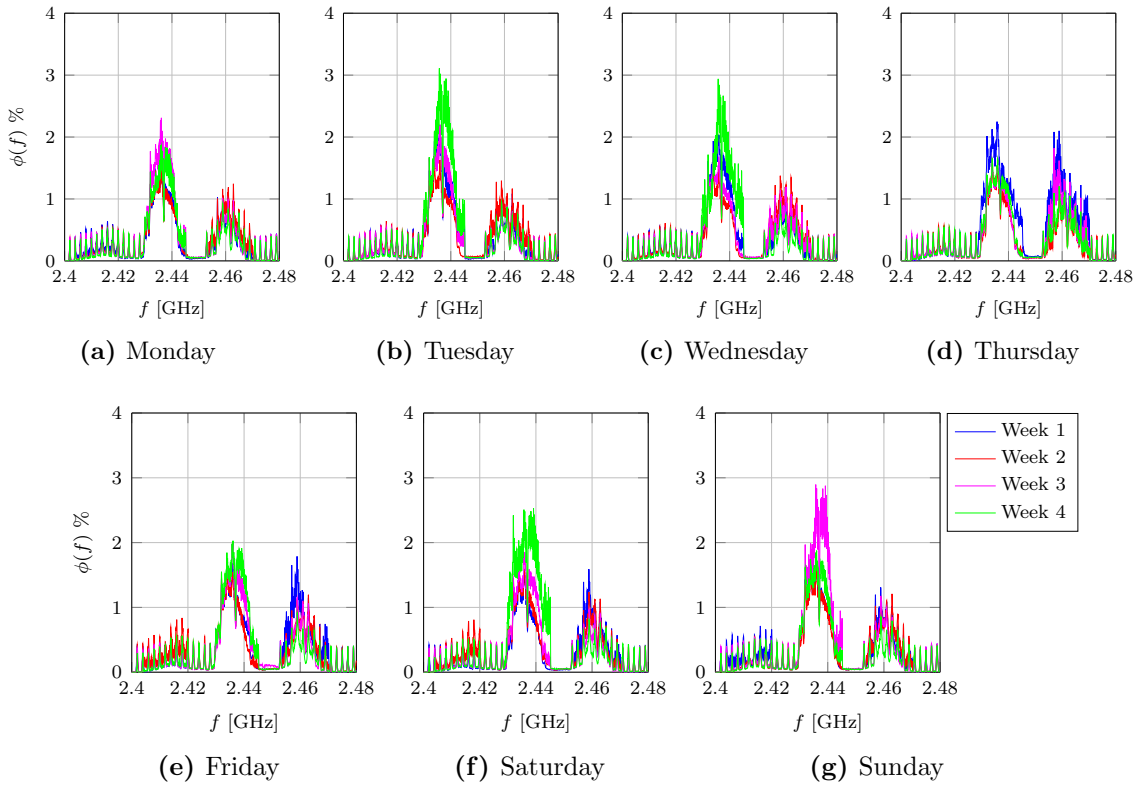

(a) Monday **(b)** Tuesday **(c)** Wednesday **(d)** Thursday

(e) Friday **(f)** Saturday **(g)** Sunday

Figure 3.2. $\phi(f_i)$ **at ICU**

by noting Week 4 activities at both locations, as illustrated by the green curve on Figure 3.1 and Figure 3.2. On Saturday (Figure 3.1(f)) and Sunday (Figure 3.1(g)) $\phi(f_i)$ was lower at RR when compared with weekdays. The same observation was not true for ICU, where $\phi(f_i)$ was higher on Saturday (Figure 3.2(f)) than on Thursday (Figure 3.2(d)). Maximum observed $\phi(f_i)$ was 5.17% at RR and 3.11% at ICU.

Correlation

To investigate the consistency of $\phi(f_i)$ during the survey period, Pearson correlation coefficient was calculated as:

$$r(D_i, D_j) = \frac{cov\,[D_i, D_j]}{\sigma_{D_i}\sigma_{D_i}} \tag{3.2}$$

where D_x is a 1×28 vector that contains ϕ readings on sub-channel $x \in [1, M]$ and $M = 1993$. r values were arranged in matrix $R^{M \times M}$ for visual representation. Consequently, matrix $P^{M \times M}$ was calculated to include p-values for testing the hypothesis of no correlation. Each p-value is the probability of a correlation as large as the observed value by random chance, when true correlation is zero. κ_x was defined as the average number of sub-channels over which a strong and statistically significant correlation has been found with sub-channel x. Strong correlation was determined when $|r(D_i, D_j)| \geq c$. Investigated values of c were 0.9, 0.8, and 0.7. Statistical significance was determined following criteria of p-value < 0.05.

$$\kappa_c(x) = \frac{1}{M} \sum_{i=1}^{M} \delta(|R_{i,x}| \geq c)\delta(P_{i,x} < 0.05) \tag{3.3}$$

where $\delta(.)$ is an indicator function that equals 1 when the condition (.) is satisfied and otherwise equals zero. Figures 3.3 and 3.4 plot R and $\kappa_c(x)$ for RR and ICU locations, respectively. RR indicated that ϕ had strong correlation (i.e., close to 1) on clusters of frequencies corresponding to IEEE 802.11 channels 1 and 11, as noted in Figure 3.3(a). Each instance of IEEE 802.11 activities occurs on a bandwidth of 20 MHz, resulting in similar CU values across the entire occupied bandwidth. Such wide-band activities exhibited significant correlation in occupancy patterns. Correlation was observed weaker on channel 6. Activities on this channel were observed to originate from both nearby and distantly deployed wireless access points. Varying detected power levels—in addition to scan-based approach used by data collection equipment—allowed more randomness in occupancy patterns that contributed to deviation from

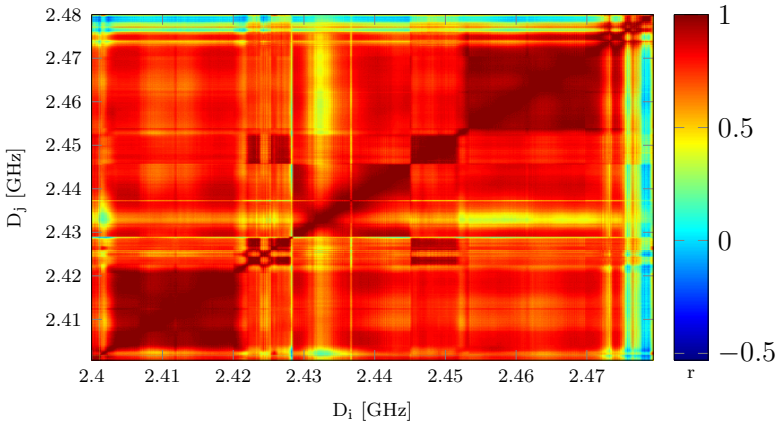

(a) R

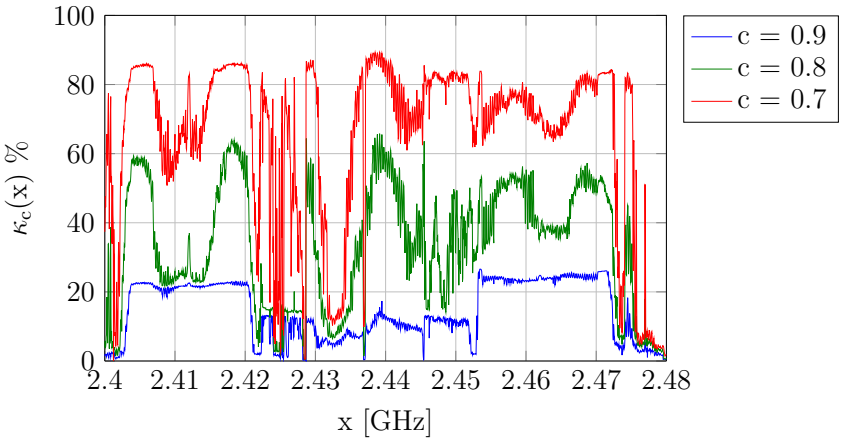

(b) $\kappa_c(x)$

Figure 3.3. Correlation of $\phi(f_i)$ at RR

linearity. Moreover, this can be realized by examining $\kappa_c(x)$ in Figure 3.3(b), where $\kappa_c(x)$ had lower values on sub-channels corresponding to channel 6 when compared to channels 1 and 11. When c value was decreased (i.e., investigated correlation strength was lower), $\kappa_c(x)$ increased to reveal a linear relationship that stretched to other sub-channels. Hence, to a certain extent—quantified by $\kappa_c(x)$—occupancy patterns on a large portion of the 2.4 GHz ISM band in RR were linearly dependent.

In the ICU, not only was there a strong correlation on channels 6 and 11, but finer clustering of high correlation values on narrow bands corresponding to BLE. Figure

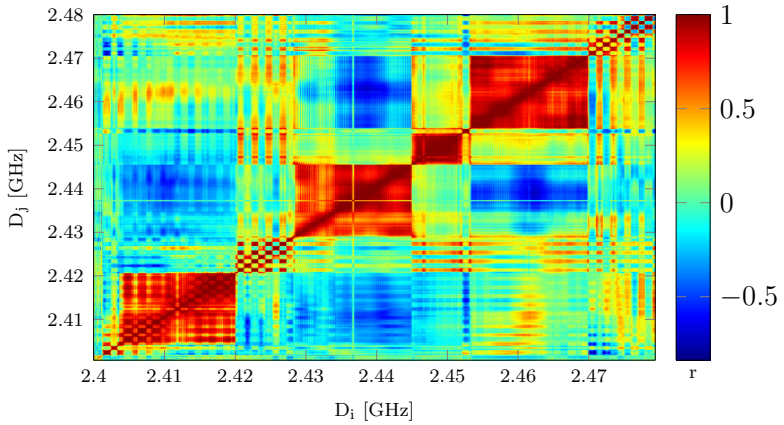

(a) R

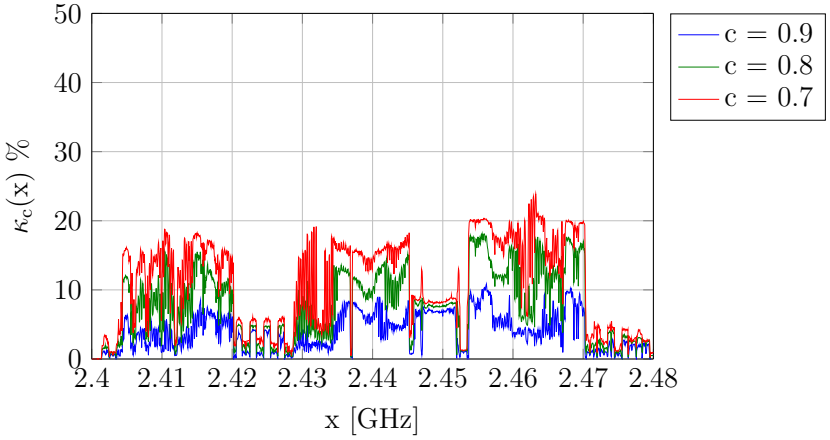

(b) $\kappa_c(x)$

Figure 3.4. Correlation of $\phi(f_i)$ at ICU

3.4(a) demonstrates that linearity was not detected outside 802.11 and BLE clusters. Changes in occupancy on a given set of sub-channels was not associated with linear change in occupancy on other sets of sub-channels, as marked by the minor increase in $\kappa_c(x)$ when c was decreased. See Figure 3.4(b).

3.4.2 CU evaluation using 1 s integration time

When IT is equal to the time necessary for acquiring a single power measurement, ϕ can have only binary values. As IT increases, more samples are depicted in the average

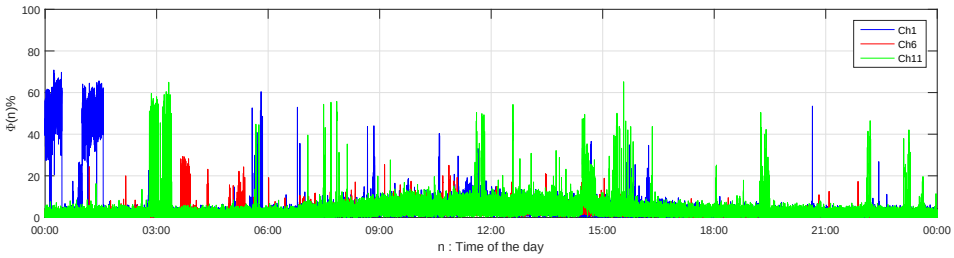

Figure 3.5. Channel utilization (Φ) variations on Wi-Fi channels 1, 6, and 11 during 24 hours. We notice that occurrences of high values are sporadic and are not concentrated in a specific time window.

Table 3.1. Model fitting parameters with 95% confidence intervals

Parameter	*Channel 1*	*Channel 6*	*Channel 11*
Shape λ_1	0.3851 (0.3842:0.386)	0.1602 (0.1597:0.1608)	0.3214 (0.3206:0.3221)
Scale λ_2	0.9286 (0.9279:0.9294)	0.7914 (0.7909:0.7919)	1.1272 (1.1264:1.1281)
Location λ_3	0.9907 (0.9899:0.9916)	1.2394 (1.2387:1.2401)	1.2463 (1.2453:1.2473)

and ϕ values become more representative of long-term spectrum occupancy. If the spectrum has periods of long inactivity, a lengthy IT will overshadow high utilization values observed sporadically in favor of low values that dominate the average. This section presents Φ_C (i.e., per second CU) for Wi-Fi channels 1, 6 and 11 at RR. The data set obtained from the completed RR spectrum survey includes approximately 6.3 M Φ_C samples for each 802.11 channel 1, 6, and 11. Φ_C is a discrete value that quantifies CU during time instance n, as defined in equation (3.1). A sample of $\Phi_{\{1,6,11\}}$ variations in a 24-hour period is depicted in Figure 3.5. Φ remains near a minimal value for most of the day with only sporadic occurrences of high activity. Findings are presented relative to the probability distribution that best fits observed Φ values in this environment. Furthermore, although Φ typically remains at the low end of possible values, cases with observed high spectrum activity are highlighted, as are instances when high values occurred during the study.

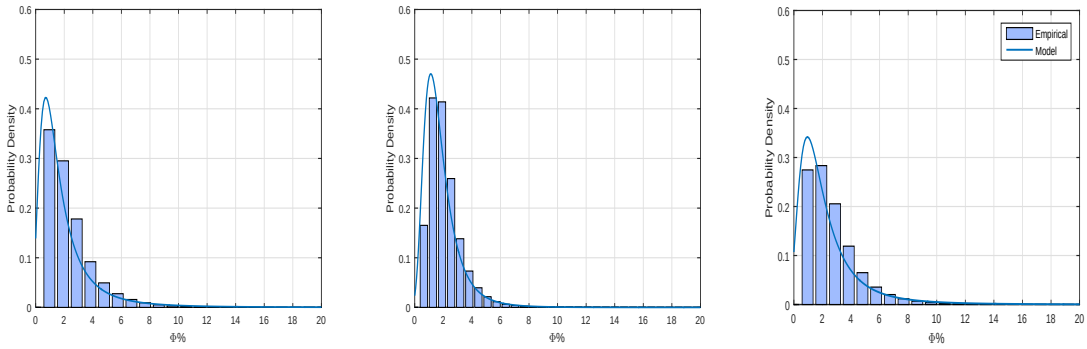

(a) Channel 1 **(b)** Channel 6 **(c)** Channel 11

Figure 3.6. Empirical and model fitted PDF of $\Phi_{\{1,6,11\}}$

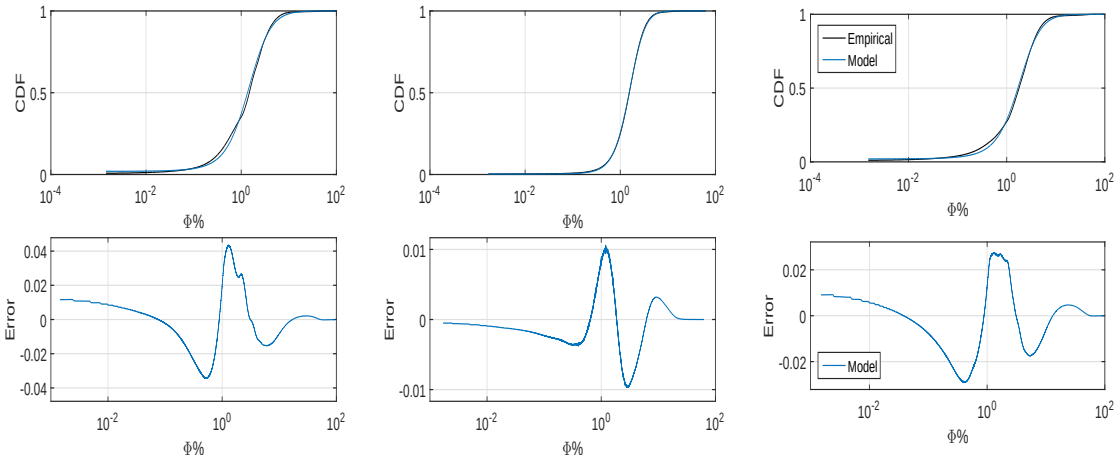

(a) Channel 1 **(b)** Channel 6 **(c)** Channel 11

Figure 3.7. Empirical and model fitted CDF and error comparison of $\Phi_{\{1,6,11\}}$

Channel utilization distribution

In addition to model fitting, empirical probability distribution functions (PDFs) of Φ are illustrated in Figure 3.6 for Wi-Fi channels 1, 6, and 11. Generalized extreme value (GEV) distribution was found to accurately fit the data based on Bayesian information criterion (BIC) when compared with a group of alternative distributions previously reported in literature as candidates for modeling CU (e.g., beta [66] and

Table 3.2. Φ Statistics

Parameter	*Channel 1*		*Channel 6*		*Channel 11*	
	Empirical	Model	Empirical	Model	Empirical	Model
Mean, μ	2.0607	2.0903	1.8523	1.8438	2.46	2.4151
Standard Deviation, σ	3.0919	3.274	1.4864	1.3246	3.6322	2.9657

t-location scale [75]). BIC is defined as

$$BIC = -2 \ln \hat{L} + k \ln n \tag{3.4}$$

where $\hat{L}$ is the maximized likelihood function of the fitted model; k is the number of estimated model parameters; and n is the total number of data points. GEV distribution is given by the density function

$$f(\Phi|\lambda_1, \lambda_2, \lambda_3) = \left(\frac{1}{\lambda_3}\right) \exp\left(-\left(1 + \lambda_1 \frac{\Phi - \lambda_2}{\lambda_3}\right)^{-\frac{1}{\lambda_1}}\right) \times \left(1 + \lambda_1 \frac{\Phi - \lambda_2}{\lambda_3}\right)^{-1-\frac{1}{\lambda_1}} \tag{3.5}$$

and is typically used to model the extremes of observation sets (e.g., maximum or minimum of repeated rounds of measurements). Mean and standard deviation of GEV are given by:

$$E[\Phi] = \mu = \lambda_2 + \frac{\lambda_3}{\lambda_1}\left(\Gamma(1 - \lambda_1) - 1\right) \tag{3.6}$$

$$\sqrt{var[\Phi]} = \sigma = \frac{\lambda_3}{\lambda_1}\sqrt{\Gamma(1 - 2\lambda_1) - \left(\Gamma(1 - \lambda_1)\right)^2} \tag{3.7}$$

where $\Gamma(x)$ is the Gamma function $\Gamma(x) = \int_0^\infty t^{x-1} e^{-t} dt$. The majority of Φ observations is concentrated at low values. Empirical and model-based cumulative distribution functions (CDFs) for $\Phi_{C=\{1,6,11\}}$ are plotted in Figure 3.7, as is the corresponding

error. Notably, 97% of Φ observations for channel 1, 99% for channel 6, and 98% for channel 11, are below 10%. Consequently, GEV is an intuitive choice to model Φ. Maximum error between empirical and GEV CDF is 4%, 1%, and 2.9% for channels 1, 6, and 11, respectively. Fitting parameters for GEV shape (λ_1), scale (λ_2), and location (λ_3) with 95% confidence intervals are reported in Table 3.1. Findings of generally low Φ values on Wi-Fi channels 1, 6, and 11 in a hospital environment conform with those observed in Finland [72], Italy [74], and the United States [13]. Notably, the use of extended integration times (e.g., minutes or days) for calculating Φ could have masked the sporadic occurrences of high Φ values. In this work, using 1 s integration time allowed reporting Φ at a much higher time resolution than earlier studies.

Even though low Φ values are observed with high probability, high Φ values eventually occurred and can be noted by the logarithmic scale plot of the Φ histogram shown in Figure 3.8. A linear relationship exists for 802.11b/g and piecewise linear for 802.11n between CU and Wi-Fi network throughput, as demonstrated in [5]. Φ observations are concentrated below $\Phi = 10\%$. Therefore, emulating a similar CU in a lab environment for coexistence testing and following the findings of [5], a Wi-Fi network can be operated at a throughput of less than 5 Mbps when protocols are 802.11g or 802.11n. On the other hand, rare occurrences of $\Phi \approx 50\%$ can be correlated to Wi-Fi transmissions at approximately 20 Mbps for 802.11g/n. While testing a medical device for wireless coexistence, interchangeable CU/throughput value of the interferer with which a device can coexist successfully is quantified. This is achieved by allowing the interferer to operate on its maximum possible throughput, which in

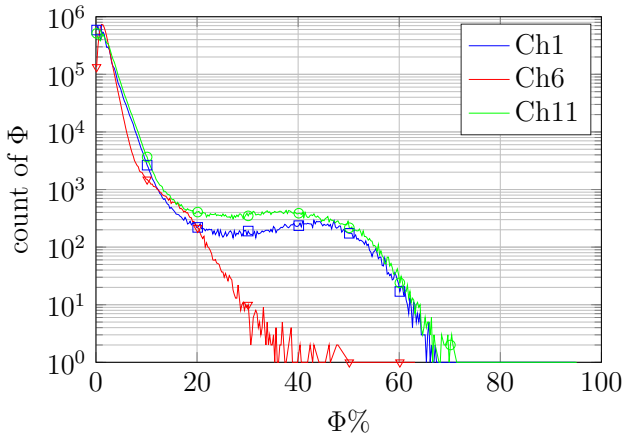

Figure 3.8. Histogram of Φ on Wi-Fi channels 1, 6, and 11. Bin width is $\Phi = 0.25\%$. Note that channel 6 exhibited considerably lower maximum values compared to channel 1 and channel 11.

turn generates the maximum possible CU. Consequently, the medical device will attempt to perform its wireless function in the presence of interference. Given failure, the interferer's throughput is reduced and the test is repeated until a CU/throughput value is found that allows successful medical device functionality. Figure 3.6, Figure 3.7, and Figure 3.8 provide an estimate of the probability of observing CU in the surveyed environment.

Temporal distribution

This section focuses on the temporal aspect of Φ (i.e., time of the day when $\Phi > \gamma$ was observed, given $\gamma\% \in [0, 99]$ is the CU value above which Φ occurrences were noted), as illustrated in Figure 3.9. Each sub-figure corresponds to one of three Wi-Fi channels investigated. Using a time bin of 60 min on the x-axis, $\zeta(n, \gamma)$ was considered the count of occurrences of $\Phi > \gamma$ in time-bin n. Logarithmic scale was used on the z-axis to avoid masking high CU values by the overwhelming number of low values.

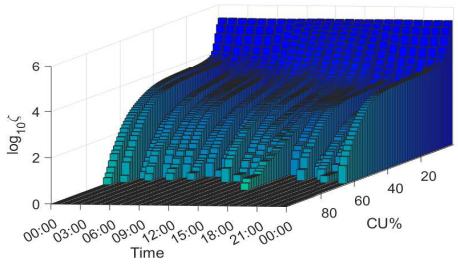

(a) Channel 1

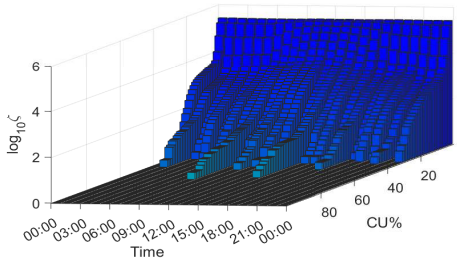

(b) Channel 6

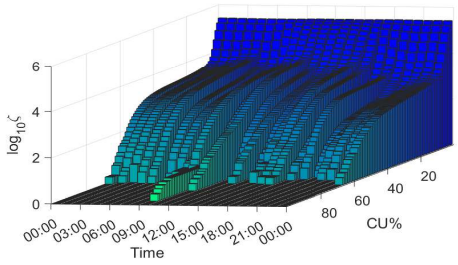

(c) Channel 11

Figure 3.9. Time distribution of $\Phi_{\{1,6,11\}}$. Time of day, n, is plotted on the x-axis, CU value, γ, above which Φ occurrences are counted, is plotted on the y-axis and $\log_{10}\zeta(n,\gamma)$ is plotted on the z-axis. High CU windows are observed during daytime (on all channels) and late night hours (on channels 1 and 11).

When investigating $\Phi > 50\%$, unique patterns were found for each studied channel. Maximum observed Φ values on channel 1 were logged at two main time windows: around midnight and between 3:00 PM and 4:00 PM. The same high spectrum usage occurred around midnight for channel 11. An intense increase in CU between 9:00 AM and 11:00 AM was also noted. As for channel 6, two high-activity windows were present between 7:00 AM and 8:00 AM, as well as between 1:00 PM and 2:00 PM. Increased activity around midnight can be attributed to either regular data upload to a central server or routine equipment software updates; daytime high activity windows can be related to human activity. These observations draw attention to the importance of estimating when a medical device is expected to operate in a hospital environment, as this knowledge directly affects the range of probable Φ values by reducing the sample set to those observed in the desired window.

Function time window

The time window used by a medical device to fulfill its wireless functions is of great importance to ensure coexistence in a realistic environment. For example, a wireless-enabled sensor might report patient vital signs to a basestation during a window of 5 s (e.g., packet holding reported data is allowed to wait in transmission queue for 5 s before it is dropped and transmission fails). Coexistence testing can be used to determine the CU below which the device can successfully perform (i.e., maximum channel temporal occupancy that allows the device to function). To achieve this, a CU value is set for each test run, and the medical device attempts to fulfill its wireless functions. Accordingly, CU integration time might be more than 1 s. In this work,

CU integration time is equal to 5 s. The medical device is deployed in the surveyed environment after Φ is empirically shown to be distributed as $f_{\Phi}(x) = Pr[\Phi = x]$, as detailed in equation (3.5) with parameters from Table 3.1. Assuming that the number of acquired samples per second is constant, Φ distribution over larger integration time of n seconds can be found by examining the random variable S_n:

$$S_n = \Phi(1) + \Phi(2) + ... + \Phi(n) \tag{3.8}$$

Consequently, $\frac{S_n}{n}$ is the CU over the larger integration time of n seconds. By the law of large numbers, we know that $\frac{S_n}{n}$ approaches mean value $\mu = E[\Phi]$ as $n \to \infty$. Mean and standard deviation for calculated and model-based Φ values are reported in Table 3.2. To quantify deviation from the mean for realistic integration times, we use the Chebyshev inequality:

$$Pr\left[\left|\frac{S_n}{n} - \mu\right| \geq \epsilon\right] \leq \frac{\sigma^2}{n\epsilon^2} \tag{3.9}$$

Figure 3.10 shows the probability of a deviation $\epsilon = 5\%$ from the mean as it approaches zero, using (μ, σ) values for channels 1, 6, and 11. See Table 3.2. Thus, it is evident that the longer a wireless device can wait to transmit, the more likely it is that CU will approximate to the mean value. In conclusion, the longer the transmission window the medical device uses to deliver data, the better the chances to successfully coexist in a realistic environment. This is true because of relatively low mean CU and random variations observed in the actual surveyed environment, as

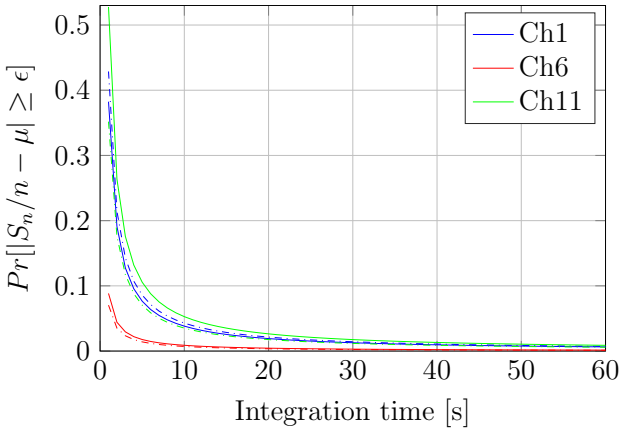

Figure 3.10. Deviation from the mean based on the Chebyshev inequality. Solid lines represent (μ, σ) obtained empirically and dashed lines for model found (μ, σ)

opposed to constant CU artificially generated in the laboratory for testing purposes, where effects on transmissions are the same regardless of device transmission window length.

3.5. Conclusion

A long-term spectrum survey in the 2.4 GHz ISM band was conducted in two healthcare facilities in the United States. A 28-day subset of survey data was first examined, and daily CU average was reported. Results showed low daily CU at a maximum of 5.17% at RR and 3.11% at ICU. Significant correlation of occupancy patterns was observed at RR for channels corresponding to IEEE 802.11 channels 1, 6, and 11. Subsequently, a statistical distribution of Wi-Fi channel utilization was derived for RR to support the healthcare community in assessing medical devices wireless coexistence. The statistical distribution GEV was found to accurately fit collected channel utilization measurements of Wi-Fi channels 1, 6, and 11. Results highlighted that 2.4

GHz wireless spectrum in the surveyed RR environment was generally lightly used with several occurrences of high channel utilization at various daytime and late-night hours. The results of this study can be used as an input to wireless coexistence testing or after-testing to estimate the probability of wireless coexistence for similar environments. However, additional RF spectrum measurement campaigns are needed in multiple hospitals and clinics, particularly those that might have higher channel utilization, to form a better picture of wireless patterns in healthcare facilities and the potential impact on medical device RF wireless coexistence. This work is being utilized to help develop a consensus standard for wireless product test methods [3], as well as a consensus technical information report on procedures to assess and manage risks associated with wireless coexistence for medical devices and systems [4].

Chapter 4: Estimating the probability of coexistence using logistic regression

4.1. Introduction

Equipping medical devices with wireless capability has become widespread. Patients and caregivers enjoy the convenience and agility these technologies offer. The wireless technology trend is expected to grow exponentially, as solutions offering an all-connected healthcare system become operational in the realm of the Internet of Things (IoT) [40]. In spite of the benefits, increased wireless device usage of unlicensed wireless spectrum bands (e.g., 2.4 GHz industrial, scientific, and medical [ISM] band) creates an urgency to ensure medical device safety and effectiveness [42]. Consequently, the U.S. Food and Drug Administration (FDA) has recommended that medical device manufacturers address wireless coexistence when applying for approval to market the device [18].

A lack of standardization for evaluating coexistence has prompted the American National Standards Institute (ANSI) ASC C63 to commence a draft of the *C63.27 Standard for Evaluation of Wireless Coexistence* [3]. Complementary to this work are efforts by the Association for the Advancement of Medical Instrumentation (AAMI)

TIR69 to prepare a standard for risk assessment of wireless coexistence for medical devices [4]. The former activity addresses coexistence testing methodology for medical and non-medical devices. The latter focuses on medical devices and addresses risk assessment of using wireless technology to perform a medical function.

Quantifying the probability of coexistence of an under-test system (UTS) in a given environment is central to the evaluation and reporting of coexistence. This is made clear in C63.27 standard draft where two tasks are identified to calculate the probability of coexistence: 1) evaluating UTS using a given test setup and, 2) incorporating electromagnetic measurements that characterize the intended deployment environment. The first task is addressed with great detail and could be attributed to either conducted or radiated testing [8]. Details about the second task can be found in our prior work (See Chapter 3 of this work and [1]), as well as in guiding documents, such as the International Telecommunication Union (ITU) report on spectrum occupancy measurement and evaluation [12]. Absent in these tasks, however, is an explanation detailing a method to aggregate the experimental evaluation of UTS into a single figure, namely the probability of coexistence (PoC). Likewise, there is no information about how to incorporate measurements from the intended environment into PoC.

4.1.1 The probability of coexistence

The FDA guidance on radio frequency wireless technology in medical devices [18] provides the following definition of wireless coexistence. The wording was informed by the IEEE 802.15.2-2003 recommended practice on coexistence of wireless personal

area networks with other wireless devices operating in unlicensed frequency bands [77]: *"the ability of one wireless system to perform a task in a given shared environment where other systems (in that environment) have an ability to perform their tasks and might or might not be using the same set of rules."*

Accordingly, an experimental setup to test wireless coexistence should include the following, as discussed in Section 2.3.2: 1) UTS (i.e., the system for which the PoC is being evaluated). Describing the UTS task or wireless function is essential to establish a clear pass/fail criteria of the test; 2) Interfering system (IS) to emulate the presence of other systems in the shared environment; and 3) Monitoring equipment (ME) to monitor test progress and outcomes. Hence, UTS PoC can be defined as the success probability of a Bernoulli random variable that tracks pass/fail status of UTS during testing (i.e., the probability that UTS successfully performs its wireless functionality under a given set of testing conditions). Logistic regression (LR) can then be used to establish the relationship between PoC and testing variables.

4.1.2 Contribution

In the literature, reports of estimating PoC are concerned with deriving the probability of failed (or successful) transmission for a given system or technology when under interference caused by another. A comprehensive list of references detailing the wireless coexistence of medical devices can be found in [6] for those running Bluetooth and in [11] for ZigBee. It is noteworthy that information in this chapter is novel because it analyzes the functional evaluation of a wireless medical device for characterizing its ability to coexist in an intended environment.

The main contribution of this chapter is proposing a framework for integrating the results of coexistence testing by utilizing LR to estimate UTS PoC. A comprehensive experimental work is presented to detail this calculation in the context of radiated open environment coexistence testing (ROECT). Explanatory variables relevant to coexistence testing were identified and tracked during the experiment. Results are presented through the study of classification accuracy of the fitted LR model. Furthermore, this work provides a model that represents the lab evaluation of a UTS. When used with the outcome of Chapter 3, UTS PoC in an intended environment is obtainable.

The balance of this chapter is organized as follows. A review of relevant work based on LR is presented in Section 4.2. Mathematical formulation of LR and a brief description of the least absolute shrinkage and selection operator (LASSO) is provided in Section 4.3. Section 4.4 details the experimental setup and data collection. Results are presented and discussed in Section 4.5. Section 4.6 concludes the chapter.

4.2. Related Work

Literature reports LR in the context of wireless communication for a number of applications, including prediction of communication quality [78–81], spectrum sensing [82], cellular networks radio resource modeling [83], location estimation [84], and enhancing energy efficiency [85]. Medical applications of LR are numerous (e.g., predicting mortality from respiratory distress [86] and tracking clinical status of heart failure patients using electrocardiography signals [87]).

In [78], authors used LR to evaluate wireless sensor network (WSN) reliability.

A reliable WSN was defined as one that covers the entire deployment region and has all nodes in the routing tree for 200 consecutive simulation cycles. The fitted model relied on two explanatory variables: transmission range and number of sensor nodes. Both were found to be statistically significant and to affect network reliability. Similarly, communication failures in a power grid distribution system were modeled using LR [79]. Model fitting was based on real-life data from Shenzhen power supply bureau in China.

When investigating the ability of communication systems to synchronize while under test in a reverberation chamber, scientists at the National Institute of Standards and Technology (NIST) used LR to investigate the extent to which coherence bandwidth and a-factor (i.e., peak-to-minimum ratio of the signal amplitude within its bandwidth) can predict system ability to demodulate a received symbol [80]. Results suggested the a-factor, being a relatively simple parameter to compute using a spectrum analyzer, is an adequate predictor of UTS behavior when compared to coherence bandwidth derived using a vector network analyzer. Liu et al. used LR as a part of their effort to design a link quality estimator for WSN [81]. The result, named 4C, relied on packet reception rate, received signal strength indicator, signal-to-noise ratio (SNR), and link quality indicator (LQI) as inputs. The output is the probability of receiving the subsequent packet. LR performance was compared to Naïve Bayes (NB) and a neural network that performs the same task. Results showed that LR offers adequate performance at low computational cost. Srivastava et al. applied LR as a classifier of spectrum availability based on investigated frequency band and observed FFT power measurements [82]. This application decreases the dependence of

spectrum sensing energy detection method on a predefined threshold. Alternatively, LR offers the probability of spectrum activity detection based on a dataset composed of prior training observations.

In an effort to optimize radio resource management (RRM) performance in LTE networks, researchers in [83] used LR to model the relationship between cellular network key performance indicators (KPIs) and RRM parameters. Subsequently, an optimization problem was solved to calculate new RRM parameters that could enhance KPIs of a given cell. The validity of the proposed model was verified by simulation. Another aspect of optimizing cellular network operations is reducing inter-cell interference (ICI) while maintaining high spectral efficiency. This can be accomplished by allocating a sub-band of spectrum resources to users on the edge of a cell that is more susceptible to ICI. To do so, a base station must decide whether user location is closer to the cell center or to the cell edge. A simplistic approach to achieve this purpose is comparing a user SINR with a predetermined threshold. Authors of [84] suggested an alternative thresholding mechanism using LR based on SINR and received power as predictors. Simulation results demonstrated that the LR model predicted user location with higher accuracy (i.e., 80% compared to 67% for SINR thresholding). With the objective of reducing energy consumption of WSN scattered in a forest, Qiang et al. used LR to model the probability of fire occurrence in a forest based on temperature and humidity readings from WSN [85]. The resulting model facilitated calculating a threshold of fire detection that was used to limit the number of transmissions of WSN nodes. Consequently, WSN energy was conserved, and WSN was operational for a longer period of time.

While previous reports in the literature have used LR for a wide variety of research objectives, the work detailed in this chapter relies on LR to provide a practical framework for calculating PoC. This information answers the needs of both industry (e.g., stakeholders [3]) and regulators (e.g., the FDA [1,18]). For device manufacturers, the presented framework could help them assess device performance under lab conditions and in real-life environments. Regulators could use results of this work as a unified and streamlined method for appraising the fitness of a given wireless device prior to market release, thus, complementing coexistence evaluation suggested in C63.27.

4.3. Mathematical formulation

During coexistence testing, the outcome y_i of a given test-run i is either pass or fail, following the definition of pass/fail criteria for the investigated wireless function and the values of explanatory variables $x_{1,i}, ..., x_{m,i}$ that characterize test-run i. Consequently, y_i is Bernoulli-distributed with success probability $\mathrm{E}[y_i|x_{1,i}, ..., x_{m,i}] = \pi_i$ and a probability mass function

$$\Pr[y_i = \gamma|x_{1,i}, ..., x_{m,i}] = \pi_i^{\gamma}(1 - \pi_i)^{1-\gamma} \tag{4.1}$$

LR aims to model π_i as a linear combination of the explanatory variables and a set of coefficients. Such a function takes values in $[-\infty, \infty]$, which is incompatible with probabilities $\in [0, 1]$. Therefore, a transformation using the logarithm of odds is implemented. The odds takes values in $[0, \infty]$, while the logarithm of odds (i.e.,

logit) takes values in $[-\infty, \infty]$.

$$logit(\pi_i) = \ln\left(\frac{\pi_i}{1-\pi_i}\right) = \beta_0 + \beta_1 x_{1,i} + ... + \beta_m x_{m,i} \tag{4.2}$$

When inversed, we find the logistic function:

$$\frac{\pi_i}{1-\pi_i} = \exp\left[\beta_0 + \beta_1 x_{1,i} + ... + \beta_m x_{m,i}\right] \tag{4.3}$$

$$\mathrm{E}[y_i | x_{1,i}, ..., x_{m,i}] = \pi_i = \frac{1}{1 + \exp\left[-\left(\beta_0 + \beta_1 x_{1,i} + ... + \beta_m x_{m,i}\right)\right]} \tag{4.4}$$

Regression coefficients can be estimated by maximizing the likelihood function:

$$L(\beta_0, ..., \beta_m) = \prod_{i=1}^{n} \pi_i^{y_i} (1-\pi_i)^{1-y_i} \tag{4.5}$$

where n is the number of observations in the dataset. Goodness of fit can be evaluated through the deviance of the fitted model, which serves as a metric to compare how well different models fit the data. Deviance D is the sum of squares of deviance residuals d_i defined as:

$$d_i = s_i \sqrt{-2\left[y_i \ln \hat{\pi}_i + (1-y_i)\ln(1-\hat{\pi}_i)\right]} \tag{4.6}$$

where $\hat{\pi}_i$ is the estimated probability of success for a given data point with a given set of regression coefficients. $s_i = 1$ if $y_i = 1$, and $s_i = -1$ if $y_i = 0$. Consequently,

deviance is:

$$D = \sum_{i=1}^{n} d_i^2 \tag{4.7}$$

Linear dependence of some explanatory variables and over-fitting could greatly increase estimated fitting coefficients, resulting in a solution that is extremely sensitive to perturbations in data. To alleviate this behavior, regularization of fitting coefficients employing LASSO could be used [88]. LASSO solves the minimization problem

$$\min_{\beta_0,\beta_1,...,\beta_m} \left(\frac{1}{n} D\left(\beta_0, \beta_1, ..., \beta_m\right) + \lambda \sum_{j=1}^{m} |\beta_j| \right) \tag{4.8}$$

where $\lambda > 0$ is a regularization parameter attempting to reach substantial goodness of fit while maintaining small-fitting coefficients. LASSO permits solutions in which some fitting coefficients are set to zero (i.e., combining coefficients estimation tasks and feature selection). Consequently, selecting the value of λ is crucial and can be accomplished by means of k-fold cross validation with different values of λ. The data set is split into k folds of equal size, and then the model is trained on all except one fold that is used for testing. Error is found as the mean of all k spared folds. Deviance can then be investigated as a function of λ; the value of minimum deviance plus one standard deviation is selected [89]. Using the selected value of λ, a regularized sparse model was built (i.e., some predictors will be zeros). With this method, some variables that contribute less to PoC can be eliminated.

4.4. Experimental setup

ROECT LOS setup was implemented in an underground laboratory at the Wireless Electromagnetic Compliance and Design Center (WECAD) at the University of Oklahoma-Tulsa. The setup layout is depicted in Figure 4.1. IS was operating IEEE 802.11n as an exemplary interfering network [6] and included two nodes: 1) access point (IS Tx) located at I_{Tx}^{IS} and 2) station (IS Rx) located at I_{Rx}^{IS}. For any given test run, IS Tx sent a stream of UDP packets at a constant configurable throughput to IS Rx. Both IS Tx and Rx were realized using Mikrotik RouterBOARD RB953GS equipped with R11e-2HPnD radio card. UTS was operating ZigBee as an exemplary technology used by medical devices and included two nodes: 1) transmitter (UTS Tx) located at I_{Tx}^{UTS} and 2) receiver (UTS Rx) located at I_{Rx}^{UTS}. For any given test run, UTS Tx attempted to transmit two packets per second. UTS wireless functionality is defined as follows: UTS Tx shall deliver at least one packet to UTS Rx during a time window of 5 s. This functionality is comparable to vital signs monitoring systems required to regularly deliver patient data to a central station or to a caregiver. Both UTS nodes were realized using Texas Instruments (TI) CC2530 development boards.

Notably, UTS nodes are considered exposed terminals. Should the objective of evaluation be to investigate the hidden terminal effect, NLOS setup could be implemented [11]. However, the ubiquitous presence of Wi-Fi networks in healthcare environments [13], in addition to the Wi-Fi deployment goal of continuous coverage, makes LOS setup more realistic. Hence, LOS is recommended in C63.27 [3]. Furthermore, the suggested method for estimating UTS PoC is not limited to ROECT.

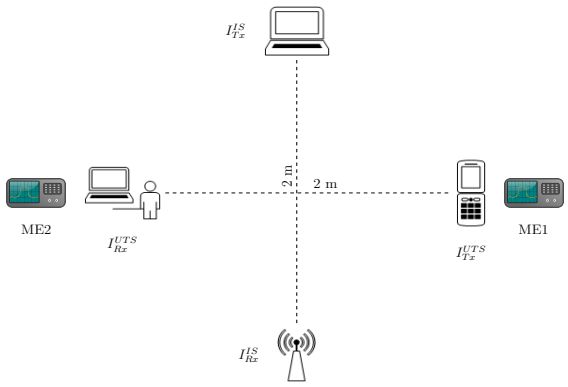

Figure 4.1. ROECT test layout.

As discussed in Section 3.1.1, coexistence testing methods attempt to characterize boundaries—in terms of fundamental wireless coexistence factors of time, frequency, and power—within which UTS operates successfully. Therefore, the integration of a testing method, other than ROECT, in the suggested framework is straightforward.

Hereafter, UTS is evaluated for wireless coexistence in time, frequency, and power by investigating several cases for each factor. Time is portrayed by IS channel utilization (CU, denoted as Φ). As such, time factor can be controlled through the configured throughput value of the IS network. Seven values of IS throughput θ^{IS} were examined and ranged from low to high values (i.e., 1 Mbps to 60 Mbps). Frequency is considered through relative allocation of center frequency and bandwidth of IS and UTS. Throughout the test, UTS occupied a static channel (i.e., ZigBee channel 17 centered at $f_c^{UTS} = 2435\ MHz$ with bandwidth $B^{UTS} = 2\ MHz$). IS was first set to occupy a co-channel relative to UTS (i.e., Wi-Fi channel 6 centered at $f_c^{IS} = 2437\ MHz$). Additionally, channels adjacent to UTS were investigated by configuring IS to operate on Wi-Fi channel 3 (centered at $f_c^{IS} = 2422\ MHz$) and then Wi-Fi channel 8 (centered $f_c^{IS} = 2447\ MHz$). Wi-Fi channels have bandwidth

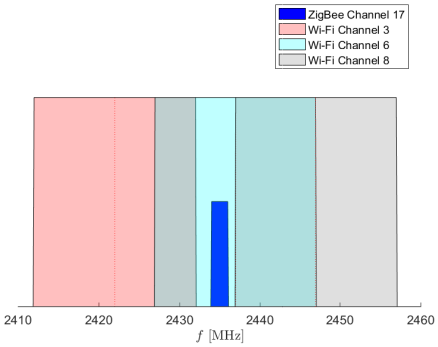

Figure 4.2. Allocation of ZigBee and Wi-Fi channels investigated in the experiment.

$B^{IS} = 20\ MHz$. Figure 4.2 illustrates the selected UTS and IS channels.

IS and UTS were evaluated at several transmission power levels. The received power at a receiver node antenna is inversely proportional to the separation distance from the transmitter node. Consequently, changing transmission power for either IS or UTS is equivalent to investigating the relative change of separation distance between the components of both systems. When IS operated on the co-channel to UTS, IS transmission power P_{Tx}^{IS} was evaluated from 16 dBm to 4 dBm with a decrement of 3 dB. When IS operated on an adjacent channel, evaluation was limited to 16 dBm and 13 dBm. Furthermore, UTS transmission power P_{Tx}^{UTS} was evaluated at 4.5 dBm, 1 dBm, -1.5 dBm, and -4 dBm.

Two devices (ME)—based on National Instruments PXIe platform—were utilized for testing. An ME was deployed 15 cm behind UTS Tx and another behind UTS Rx. When IS was operating on a co-channel to UTS, ME1 was used to obtain CU measurements of both IS and UTS, as detailed in Chapter 2. When IS was operating on an adjacent-channel to UTS, ME1 was used to monitor wireless activity in time

domain on the channel occupied by UTS. Similarly, ME2 was used to monitor wireless activity on the channel occupied by IS. Post processing of power measurement data was accomplished by applying an activity detection threshold fixed at three standard deviations above the noise mean, as demonstrated in Section 2.4.1. This allowed estimation of Φ values for both IS and UTS on their respective channels.

A total of 252 test vectors were inspected. Each test vector was executed for 2 minutes. Given that the wireless function of UTS is defined over 5 s, 24 data points per test vector were generated. Consequently, a dataset of 6048 data points was obtained. For each observation i, the following explanatory variables were recorded: $P_{Tx,i}^{IS}$, Φ_i^{IS}, θ_i^{IS}, $P_{Tx,i}^{UTS}$, Φ_i^{UTS}, $f_{c,i}^{IS}$, B_i^{IS}, $f_{c,i}^{UTS}$, and B_i^{UTS}. Additionally, variable y_i was recorded, which is a binary indicator that equals 1 if UTS Rx received at least one packet during a time window of 5 s; otherwise, $y_i = 0$. To unify the explanatory variables that pertain to the operating frequency of IS and UTS, $\Delta\left(f_c^{IS}, B^{IS}, f_c^{UTS}, B^{UTS}\right)$ is introduced as a distance metric between the UTS and IS channels.

$$\Delta = \begin{cases} \exp\left(\frac{-1}{\left(f_c^{UTS} - \frac{B^{UTS}}{2}\right) - \left(f_c^{IS} + \frac{B^{IS}}{2}\right)}\right) & \text{if } \left(f_c^{IS} + \frac{B^{IS}}{2}\right) < \left(f_c^{UTS} - \frac{B^{UTS}}{2}\right) \\ \exp\left(\frac{-1}{\left(f_c^{IS} - \frac{B^{IS}}{2}\right) - \left(f_c^{UTS} + \frac{B^{UTS}}{2}\right)}\right) & \text{if } \left(f_c^{IS} - \frac{B^{IS}}{2}\right) > \left(f_c^{UTS} + \frac{B^{UTS}}{2}\right) \\ 0 & \text{otherwise} \end{cases} \tag{4.9}$$

When IS and UTS channels overlap, $\Delta = 0$. The further IS channel edge is from UTS channel edge, $\Delta \longrightarrow 1$. Figure 4.3 plots Δ in the case of ZigBee UTS operating at channel $f_c^{UTS} = 2435\ MHz$ with bandwidth $B^{UTS} = 2\ MHz$. IS is a Wi-Fi system with $B^{IS} = 20\ MHz$ on any of the 13 possible channels in the 2.4 GHz ISM band.

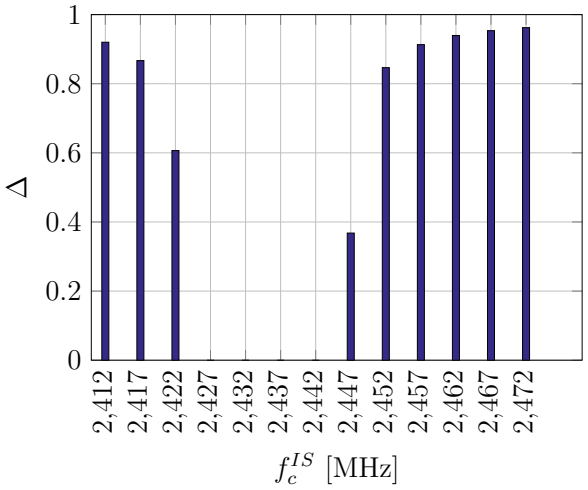

Figure 4.3. Distance metric between IS and UTS channels $\Delta\left(f_c^{IS}, B^{IS}, f_c^{UTS}, B^{UTS}\right)$

4.5. Results

Exploratory data analysis was performed to draw insight about the relationships between explanatory variables. Afterwards, LR model fitting using LASSO was detailed, and then selected features were used in an LR model using least square fit. The model's ability to accurately classify test cases and predict pass/fail outcome was evaluated. Finally, results were used in tandem with those reported in Section 3.4.2 to simulate and present UTS PoC in a hospital environment.

4.5.1 Exploratory Analysis

It has been established that there is a piecewise-linear relationship between 802.11n Φ and θ (See [5] and Section 2.4.1). Figure 4.4 confirms that the observed behavior of Φ^{IS} as a function of θ^{IS} follows the same trend. Linear increase in Φ is caused by transmitter channel access for frame transmissions and receiver response through acknowledgments. Once frame aggregation of 802.11n is exploited to achieve high θ,

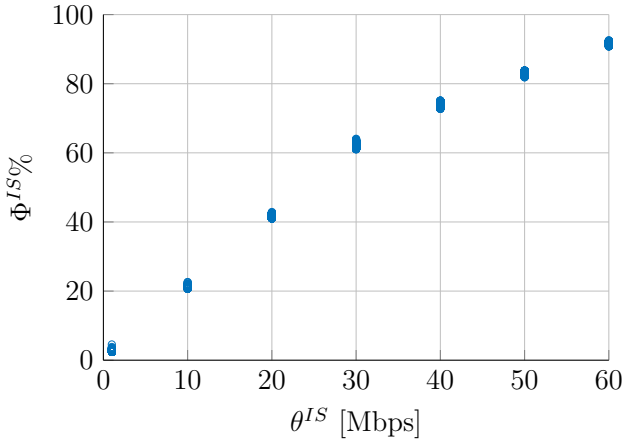

Figure 4.4. Φ^{IS} as a function of θ^{IS}

longer frames are sent through the channel with less frequent acknowledgments. This explains the smaller slope of the $\Phi(\theta)$ curve.

To fulfill its wireless function, UTS must achieve a certain Φ. Coexistence factors could affect Φ^{UTS} and deprive UTS from gaining channel access. Figure 4.5 plots Φ^{UTS} as a function of P_{Tx}^{IS}. Logarithmic scale is used on the y-axis to account for the fact that Φ^{UTS} exhibits low values (0.15% on average). It is evident that when P_{Tx}^{IS} is low (i.e., IS is at a further distance from UTS), Φ^{UTS} remains at nearly the average value, indicating that UTS was able to gain the required Φ. When P_{Tx}^{IS} becomes high (e.g., 14 dBm and 16 dBm), the spread of Φ^{UTS} values is more evident. When IS signal is transmitted with ample power for detection at UTS Tx antenna, UTS Tx will defer its transmission until the channel becomes available. Consequently, UTS Tx is deprived from channel access until there is adequate spectrum opportunity to transmit—following the rules of CSMA/CA, which in turn contributes to higher variability of Φ^{UTS}. Notably, P_{Tx}^{IS} does not independently explain the behavior of Φ^{UTS}. Φ^{UTS} was plotted as a function of Φ^{IS} for each studied P_{Tx}^{IS} on Figure 4.6. Figure

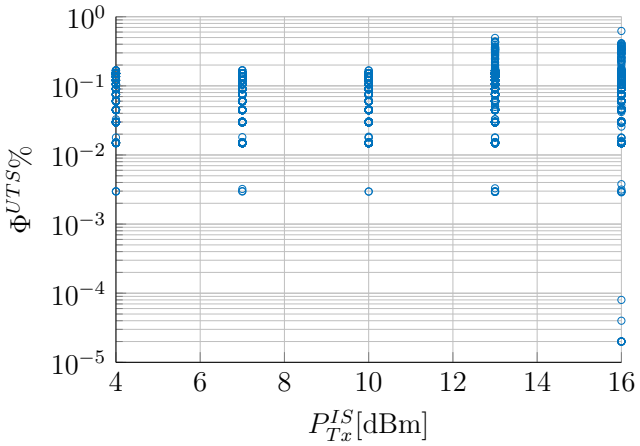

Figure 4.5. Φ^{UTS} **as a function of** P_{Tx}^{IS}

4.6(b) illustrates when IS occupies a co-channel to UTS; Figure 4.6(a) and Figure 4.6(c) portray IS adjacent-channels. For each investigated θ^{IS} value, $\left(\Phi^{IS}, \Phi^{UTS}\right)$ data points are placed on the scatter plot using small dots. Large dots connected with straight lines represent average Φ^{IS} and Φ^{UTS} observed for each θ^{IS}. Figure 4.6(b) indicates that Φ^{UTS} decreases when Φ^{IS} increases. Spectrum sharing between Wi-Fi and ZigBee on a co-channel favors Wi-Fi transmissions; ZigBee experiences increased packet loss [90]. Furthermore, average Φ^{UTS} decreases when P_{Tx}^{IS} increases for a given θ^{IS}. This trend validates observations in Figure 4.5. Although Wi-Fi channels 3 and 8 are adjacent to ZigBee channel 17, Wi-Fi channel 8 is closer to ZigBee channel 17 when compared with Wi-Fi channel 3 (i.e., 1 MHz separation band between the two channel edges as opposed to 2 MHz). Using Equation 4.9, $\Delta = 0.36$ for Wi-Fi channel 8 and $\Delta = 0.6$ for Wi-Fi channel 3, indicating shorter separation distance. Consequently, filter imperfections are more pronounced when IS is operating on channel 8, as demonstrated by comparing Figure 4.6(c) with Figure 4.6(a). The higher θ^{IS}, the higher Φ^{IS}, which increases the chance that RF energy leaked to

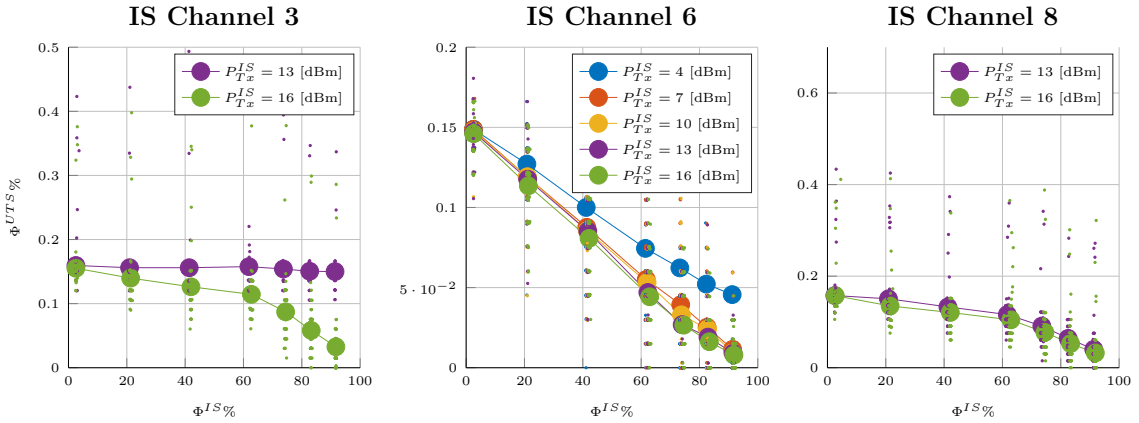

(a) Lower adjacent-channel **(b)** Co-channel **(c)** Upper adjacent-channel

Figure 4.6. Φ^{UTS} **as a function of** Φ^{IS}

the adjacent band might be detected by UTS (hence, lower Φ^{UTS} observed at high values of θ^{IS}). Notably, when $P_{Tx}^{IS} = 13\ dBm$ (See Figure 4.6(a)), Φ^{UTS} remains constant regardless of θ^{IS}. In this case, energy leakage is not ample for UTS to detect or to corrupt UTS transmissions.

4.5.2 Model fitting and performance

To generate training and testing datasets, a stratified sampling procedure was used to ensure that the percentage of records per class (i.e., pass or fail) was respected in both training and testing datasets. Sixty percent of the dataset was selected for training, and the remaining 40% for testing.

Fitting using LASSO

To determine the regularized regression coefficients β, a value for the regularization parameter λ in Equation 4.8 must be selected. Figure 4.7 demonstrates this process through 10-fold cross validation with different values of λ. Accordingly, deviance was

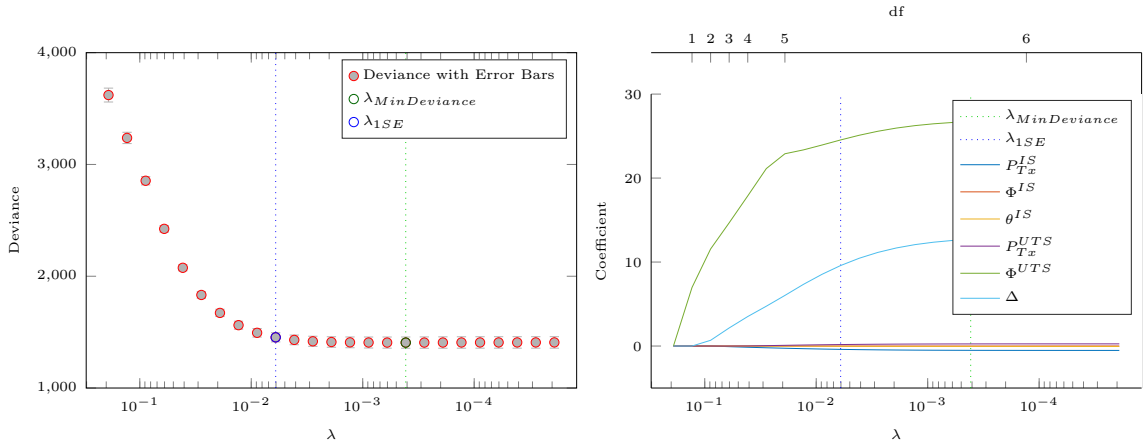

(a) Cross-validated deviance **(b)** Trace plot of coefficients fit

Figure 4.7. Selection of the regularization parameter λ

inspected as a function of λ, as illustrated in Figure 4.7(a). The value of λ with minimum deviance plus one standard deviation was then selected [89]. A trace plot is presented in Figure 4.7(b) to demonstrate the decrease of regression coefficients values when λ increases. Given the largest λ, all coefficients diminish to zero. LASSO eliminated Φ^{IS} by assigning a corresponding zero coefficient while also allowing its linearly-dependent variable θ^{IS} to remain in the fit. Coefficients estimate is presented in Table 4.1. Notably, Φ^{UTS} and Δ are associated with the largest coefficients, indicating that a small change in either variable is connected to a large change in log odds. P_{Tx}^{IS} has a negative coefficient, implying that log odds decrease when P_{Tx}^{IS} increase (or, conversely, separation distance between IS and UTS decreases). The opposite is true for P_{Tx}^{UTS}. An increase in θ^{IS} yields a decrease of log odds, as indicated by the negative associated coefficient.

Table 4.1. Regularized regression coefficients

Variable	(Intercept)	P_{Tx}^{IS}	Φ^{IS}	θ^{IS}	P_{Tx}^{UTS}	Φ^{UTS}	Δ
Coefficient Estimate	4.9740	-0.4182	0	-0.0328	0.2030	24.9900	10.4920

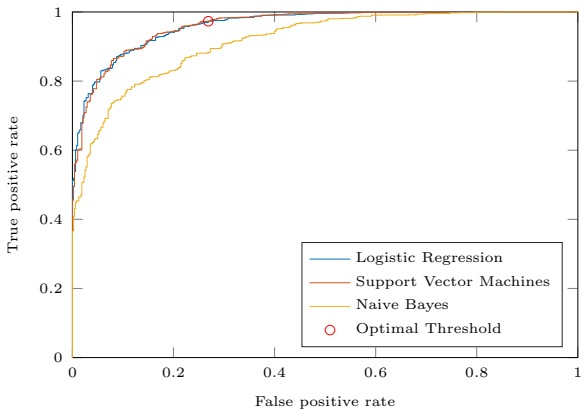

Figure 4.8. ROC Curves for LR, SVM, and NB classifiers

The regularized logistic regression model was then evaluated on the test dataset. Model classification performance relative to receiver operating characteristic (ROC) curve was compared with NB and Support Vector Machine (SVM) classifiers. NB is a simple probabilistic classifier attempting to predict the most probable outcome based on accumulated training information. SVM relies on the training dataset to look for an optimal hyperplane for separating the two investigated classes with the maximum margin in order to minimize classification error. Figure 4.8 shows a comparison between LR, SVM, and NB—all of which were trained using the same dataset. LR exhibited the highest area-under-the-curve (AUC = 0.9621), which was slightly higher than linear SVM (AUC = 0.9618). NB exhibited the lowest AUC (i.e., 0.9158). In spite of the fact that LR and SVM performance was extremely close, LR is favorable, given the interpretability of fitted coefficients, which contributes to better understanding of coexistence testing results and allows targeted development of UTS, if needed.

Finally, optimal threshold for maximizing LR classification accuracy is selected, and model performance is evaluated on the testing dataset, accordingly. Results of

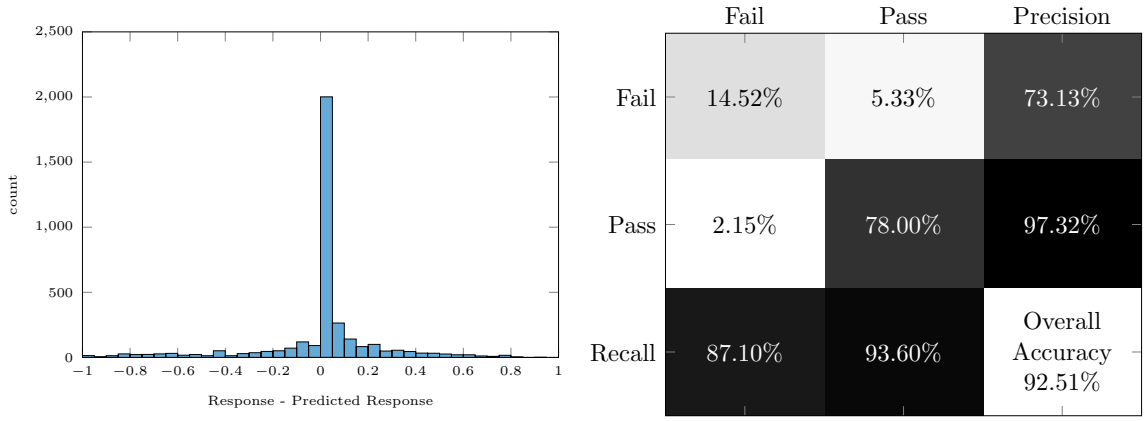

(a) Residuals **(b)** Confusion matrix

Figure 4.9. Performance of LASSO estimated model

the evaluation are presented using a residual plot and confusion matrix (See Figure 4.9). A preliminary evaluation of fitted model prediction performance using the training dataset is presented through the residuals plot on Figure 4.9(a). Note that the majority of residuals is concentrated close to zero, indicating favorable expected performance of the fitted model for estimating PoC and predicting a test-case outcome. Overall accuracy of the LASSO regularized model was 92.51%, as shown in Figure 4.9(b). For "Pass" class of coexistence testing, the model exhibited an F-score[1] of 95.42%. F-score for "Fail" class was 78.30%, although 87.10% of these cases were accurately labeled as part of the "Fail" class.

Statistical significance

Bootstrapping (i.e., repeated sampling) could be used to obtain standard error (SE) distribution for estimated regularized coefficients. However, SE of regularized coefficients was not calculated because penalization by λ introduces bias to the esti-

[1] $F = 2 \times \frac{p \times r}{p+r}$ where p is the precision and r is the recall.

Table 4.2. Least square coefficient estimates for non-zero explanatory variables determined by LASSO

Variable	*Estimate*	*SE*	*z-value*	*p-value*
(Intercept)	6.4899	0.5481	11.840	2.4266e-32
P_{Tx}^{IS}	-0.5158	0.0257	-20.062	1.5773e-89
θ^{IS}	-0.0482	0.0079	-6.034	1.5932e-09
P_{Tx}^{UTS}	0.2695	0.0250	10.776	4.4553e-27
Φ^{UTS}	26.775	3.1822	8.414	3.9601e-17
Δ	13.175	0.7119	18.505	1.8674e-76

mate [91, 92]. Therefore, results obtained from bootstrapping provide only an approximate picture for SE behavior. Alternatively, LASSO is considered as a feature selection phase. Accordingly, explanatory variables with non-zero coefficients were used as input to least-square (LS) fitting to obtain estimates for which SE, z-value, and p-value were established. Table 4.2 details LS coefficient estimates of non-zero explanatory variables determined by LASSO. For each coefficient β_j, z-value is calculated as β_j/SE_j. All z-values have a magnitude > 2. Consequently, p-values are $<$ 0.05, indicating that all investigated explanatory variables are statistically significant. LS estimated model performance—based on optimal threshold obtained by ROC—by means of residuals plot and confusion matrix is illustrated in Figure 4.10. Notably, the majority of residuals was near zero (See Figure 4.10(a)). Overall accuracy of LS model is illustrated in Figure 4.10(b) and determined at 92.72%, slightly higher than that of the LASSO model (See Figure 4.9(b)). For "Pass" class, the model exhibited an F-score of 95.57%. F-score for "Fail" class was 79.53%. Ninety percent of "Fail" test cases were labeled accuratelyz.

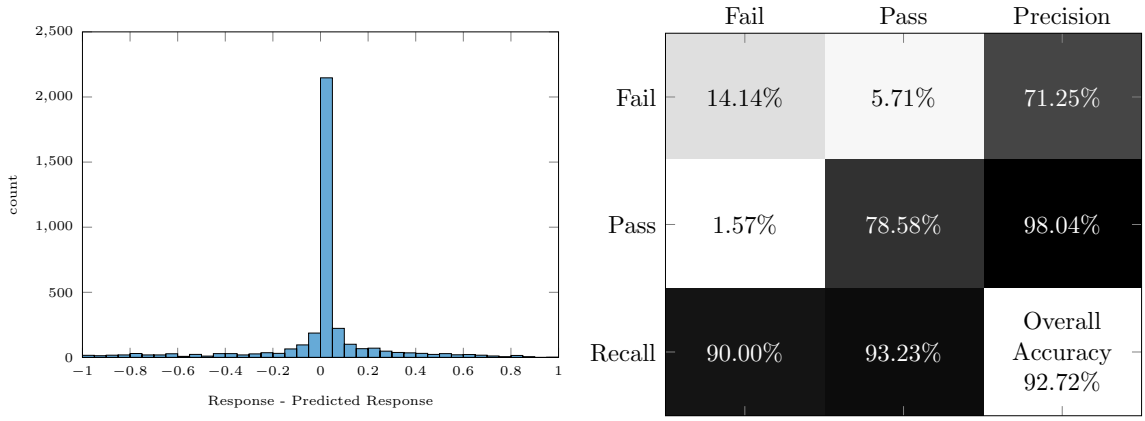

(a) Residuals **(b)** Confusion matrix

Figure 4.10. Performance of LS estimated model

4.5.3 UTS PoC in deployment environment

The model detailed in Equation 4.4 with coefficients reported in Table 4.2 permits UTS PoC estimation for a given set of explanatory variables. However, to estimate UTS PoC *in a given intended environment*, statistical distribution representing Φ^{IS} values expected in the environment must be incorporated. In Section 3.4.2, Φ data were fitted to a generalized extreme value (GEV) distribution with parameters detailed in Table 3.1. Consequently, Monte Carlo simulation was constructed to draw random Φ^{IS} values from GEV distribution that represent co-channel IS behavior in a post-surgery recovery room (RR) environment. Afterwards, Φ^{IS} values were converted into θ^{IS} that could be used with LR model. To do so, linear interpolation was used to estimate θ^{IS} using data points, as illustrated in Figure 4.4. Notably, GEV distribution was utilized for Φ with 1 s integration time. However, UTS wireless functionality was defined over 5 s. Therefore, for each simulation iteration, five Φ^{IS} values were drawn, and the mean was used for the following steps.

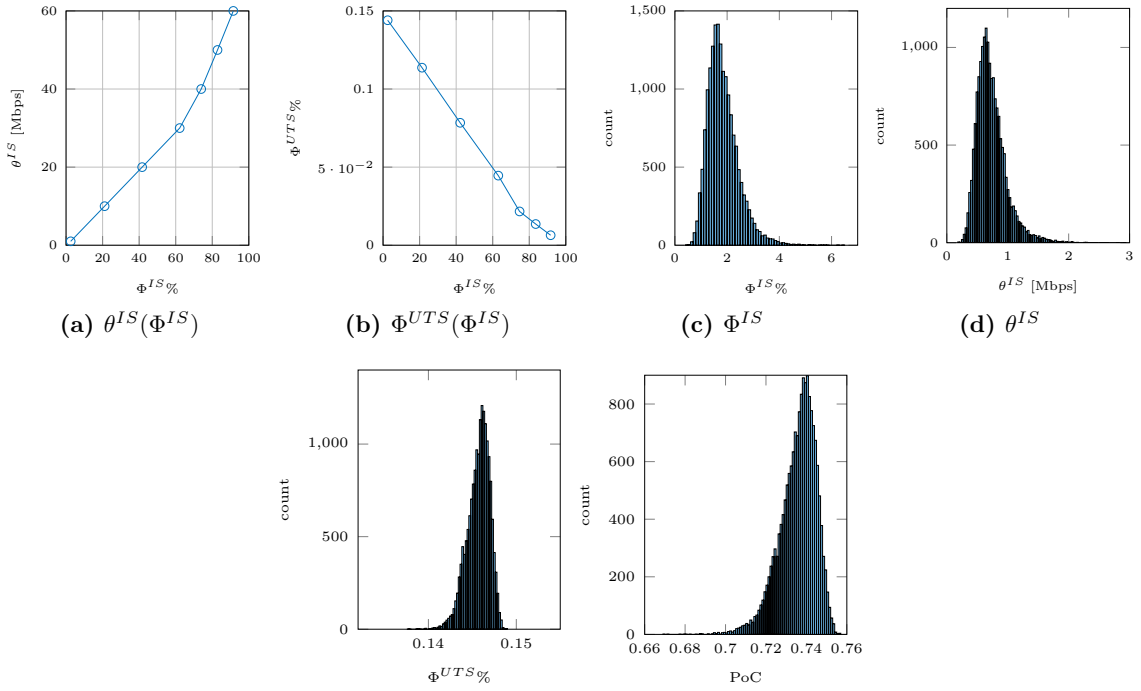

(a) $\theta^{IS}(\Phi^{IS})$ **(b)** $\Phi^{UTS}(\Phi^{IS})$ **(c)** Φ^{IS} **(d)** θ^{IS}

(e) Φ^{UTS} **(f)** PoC

Figure 4.11. Simulation variables

During the simulation, IS was assumed to operate statically on co-channel to UTS (i.e., Wi-Fi channel 6). Hence, $\Delta = 0$. Moreover, P_{Tx}^{IS} and P_{Tx}^{UTS} were assumed constant. Figure 4.6 demonstrates that Φ^{UTS} decreases as Φ^{IS} increases. Therefore, simulated Φ^{IS} were used to estimate expected Φ^{UTS} (for a given P_{Tx}^{IS} and P_{Tx}^{UTS}) using linear interpolation. The simulation was run for 17280 iterations (i.e., representative of a 24-hour operation for UTS in its intended environment). Figure 4.11 illustrates the curve used to estimate θ^{IS} (See Figure 4.11(a)) and Φ^{UTS} (See Figure 4.11(b)) based on Φ^{IS}, given that $P_{Tx}^{IS} = 16$ dBm and $P_{Tx}^{UTS} = -4$ dBm. Additionally, histograms are plotted on Figures 4.11(c)-(f) to demonstrate exhibited values of Φ^{IS}, θ^{IS}, Φ^{UTS}, and PoC during the simulation.

Finally, the mean and 99% confidence interval[2] of UTS PoC for all investigated P_{Tx}^{IS} and P_{Tx}^{UTS} values were calculated and are illustrated in Figure 4.12. Reported PoC values can be interpreted, as follows. When UTS is deployed in the RR environment and separation distance between UTS nodes and UTS/IS is represented by P_{Tx}^{UTS} and P_{Tx}^{IS}, respectively, UTS is expected to execute its wireless functionality during a 24-hour period with a success probability of PoC. Note that UTS PoC in RR environment decreases for a given P_{Tx}^{UTS} when P_{Tx}^{IS} increases. When P_{Tx}^{UTS} is at its lowest (i.e., furthest deployment of UTS Tx and Rx) and P_{Tx}^{IS} at its highest (i.e., closest distance between UTS and IS), UTS PoC was estimated at 73.56%. Whether this value estimates acceptable performance for UTS follows the risk assessment of UTS wireless functionality (See [4]).

Consequently, surveying the intended environment RF spectrum and carefully selecting UTS RF parameters during deployment will contribute greatly to enhancing operational UTS PoC.

4.6. Conclusion

The use of logistic regression to estimate the probability of coexistence of a UTS has been suggested and implemented. The probability of coexistence was first defined by analyzing the definition of wireless coexistence using text from regulatory bodies. Radiated open environment coexistence testing was then used to realize a test scenario in which IS was 802.11n and UTS was ZigBee (i.e., exemplary technologies for

[2]calculated as $\mu \pm 2.58\frac{\sigma}{\sqrt{n}}$, where μ is the sample mean, σ is the sample standard deviation, and n is the number of samples.

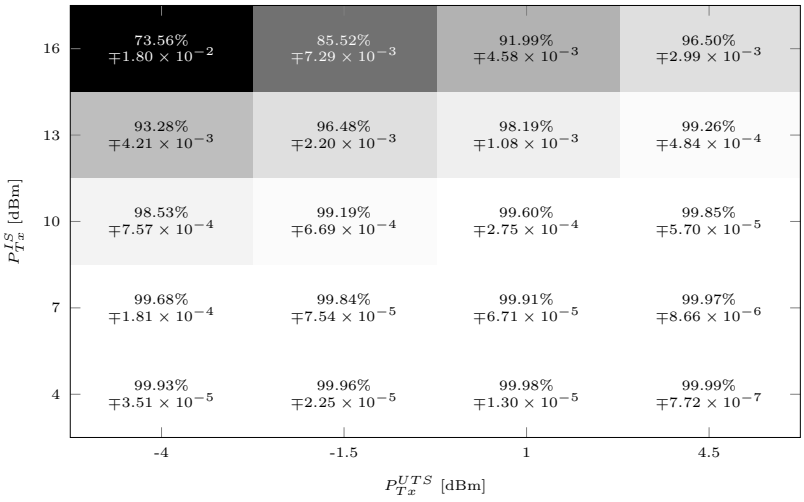

Figure 4.12. UTS probability of coexistence in RR

interfering network and medical device, respectively). LASSO was used to fit a regularized LR model that exhibited high overall accuracy of classification on a testing dataset that included the outcome of a wide variety of coexistence testing scenarios. The reduced set of explanatory variables was then used to fit an LR model that exhibited the same trend of accuracy. Finally, results were incorporated with findings from Chapter 3 in the form of Monte Carlo simulation to estimate UTS probability of coexistence in a hospital environment.

Chapter 5: Conclusion and future work

This dissertation addresses a number of practical topics that are central to the evaluation and reporting of wireless coexistence, primarily for wireless-enabled medical devices.

Testing methods currently under consideration as part of a consensus standard for coexistence evaluation were summarized and compared. A novel method for estimating channel utilization of multiple coexisting wireless systems was developed using machine-learning techniques. The suggested method is especially helpful in radiated open environment coexistence testing. Upon validation, overall accuracy was determined at 98.86%. Two case-studies were introduced to observe how collocated systems interact while sharing spectrum resources. Findings of observed performance for 802.11n and ZigBee systems conform with those reported in literature.

Typical electromagnetic environments for medical device usage were investigated. A long-term spectrum survey of the 2.4 GHz ISM band was conducted in two healthcare facilities. Daily channel utilization average was inspected to reveal regularly used channels. Results showed low utilization values. Significant correlation of occupancy patterns was observed for channels corresponding to Wi-Fi channels 1, 6, and 11. Accordingly, statistical distribution GEV was found to accurately fit collected chan-

nel utilization measurements for Wi-Fi channels 1, 6, and 11. Results highlighted that in the surveyed environment, the 2.4 GHz ISM wireless spectrum was generally used quite lightly with several occurrences of high channel utilization used at various daytime and late-night hours.

A statistical framework based on logistic regression was detailed to serve as the outcome of coexistence testing reports and estimate the probability of coexistence. Framework use was demonstrated through a typical testing scenario that utilized 802.11n for IS and ZigBee for UTS. Given probable linear-dependence between explanatory variables, LASSO was used as a feature selection phase. Consequently, a logistic regression fit using the reduced set of variables was calculated. The fitted model was highly accurate in predicting the outcome of a wide variety of test scenarios. Results were used together with those of the spectrum survey in a Monte Carlo simulation to estimate UTS coexistence probability in its intended use environment.

5.1. Future work

The spectrum survey reported in Chapter 3 was performed at static locations in the surveyed environment. Future work would include the development, realization, and deployment of a distributed spectrum survey system. Such a system would comprise low-cost distributed nodes that estimate and report local CU readings. Online processing would alleviate the need to store high volumes of data. Data would be incorporated to establish a spatial CU distribution (i.e., a distribution of CU values on a given frequency band at a given location). In this case, results reported in Chapter 4 could be leveraged to estimate coexistence probability at several locations. Fur-

thermore, based on preliminary work to model CU in space by integrating localized readings [63, 93], mobility scenarios could be introduced to the assessment of wireless coexistence. If low-cost implementation of sensing nodes was achieved, large-scale (i.e., multiple environments) surveys could lead to a reference database of spectrum activity status in healthcare environments.

UTS CU proved to be an important factor for evaluating wireless coexistence, as demonstrated in Chapter 4. Work presented in Chapter 2 could be extended to address frequency-hopping systems (e.g., Bluetooth and BLE). A metric representing channel time occupancy while hopping would be researched and defined. Accordingly, adequate wide-band hardware implementation would be executed to capture spectrum activity at rates higher than Bluetooth hopping rate (i.e., 1600 hops per second). Consequently, Bluetooth channel occupancy would be quantified and investigated.

Work presented in this dissertation was primarily applied to wireless coexistence of medical devices. However, researched concepts and methods are relevant to an increasingly expanding list of domains, including automotive (e.g., infotainment systems, mobile phones, and in-vehicle sensor network); cellular (e.g., testing and development of cellular extensions in unlicensed bands like Licensed-Assisted Access [LAA]); and industrial.

Bibliography

[1] M. O. Al Kalaa, W. Balid, H. H. Refai, N. J. LaSorte, S. J. Seidman, H. I. Bassen, J. L. Silberberg, and D. Witters, "Characterizing the 2.4 GHz Spectrum in a Hospital Environment: Modeling and Applicability to Coexistence Testing of Medical Devices," *IEEE Transactions on Electromagnetic Compatibility*, vol. 59, no. 1, pp. 58–66, feb 2017.

[2] Marketsandmarkets.com, "Wireless Devices Market for Medical by Technology (BT/BLE, Wi-Fi, ZigBee, ANT+), Component (Sensors, ICs, Processors), Application (Monitoring, Medical Therapeutics, Diagnosis, Fitness & Wellness), and Geography – Global Forecast to 2020 [SE 3039]," Tech. Rep., 2014.

[3] American National Standards Institute (ANSI) ASC C63, "C63.27 Standard for Evaluation of Wireless Coexistence [In development]."

[4] Association for the Advancement of Medical Instrumentation (AAMI) TIR69, "Risk Assessment of radio-frequency wireless coexistence for medical devices and systems [In development]," 2016.

[5] S. A. Rajab, W. Balid, and H. H. Refai, "Comprehensive study of spectrum occupancy for 802.11b/g/n homogeneous networks," in *2015 IEEE International Instrumentation and Measurement Technology Conference (I2MTC) Proceedings*. IEEE, may 2015, pp. 1741–1746.

[6] S. Seidman and N. LaSorte, "An experimental method for evaluating wireless coexistence of a Bluetooth medical device," *IEEE Electromagnetic Compatibility Magazine*, vol. 3, no. 3, pp. 49–54, 2014.

[7] N. J. LaSorte, D. Bloom, S. Rajab, and H. H. Refai, "Creating an automated and emulated 802.11g wireless interfering network for wireless coexistence testing," in *2013 IEEE International Instrumentation and Measurement Technology Conference (I2MTC)*. IEEE, may 2013, pp. 1022–1027.

[8] W. F. Young, J. B. Coder, and L. A. Gonzalez, "A review of wireless coexistence test methodologies," in *2015 IEEE Symposium on Electromagnetic Compatibility and Signal Integrity*. IEEE, mar 2015, pp. 69–74.

[9] G. Manzi, M. Feliziani, P. a. Beeckman, and N. van Dijk, "Coexistence between ultra-wideband radio and narrow-band wireless LAN communication systems -

Part II: EMI evaluation," *IEEE Transactions on Electromagnetic Compatibility*, vol. 51, no. 2, pp. 382–390, 2009.

[10] K. A. Remley and W. F. Young, "Test methods for RF-based electronic safety equipment: Part 2 — Development of laboratory-based tests," *IEEE Electromagnetic Compatibility Magazine*, vol. 2, no. 1, pp. 70–80, 2013.

[11] N. J. LaSorte, S. A. Rajab, and H. H. Refai, "Developing a reproducible non-line-of-sight experimental setup for testing wireless medical device coexistence utilizing ZigBee." *IEEE transactions on bio-medical engineering*, vol. 59, no. 11, pp. 3221–9, nov 2012.

[12] ITU-R, "Spectrum occupancy measurements and evaluation," *SM Series Report ITU-R SM.2256*, vol. 2256, no. July, 2012.

[13] M. O. Al Kalaa, G. Butron, W. Balid, H. H. Refai, and N. J. LaSorte, "Long term spectrum survey of the 2.4 GHz ISM band in multiple hospital environments," in *2016 IEEE Wireless Communications and Networking Conference Workshops (WCNCW)*. IEEE, apr 2016, pp. 246–251.

[14] "IEEE Standard for Information technology– Local and metropolitan area networks– Specific requirements– Part 11: Wireless LAN Medium Access Control (MAC)and Physical Layer (PHY) Specifications Amendment 5: Enhancements for Higher Throughput," pp. 1–565, 2009.

[15] "IEEE Standard for Information Technology - Telecommunications and Information Exchange Between Systems - Local and Metropolitan Area Networks Specific Requirements Part 15.4: Wireless Medium Access Control (MAC) and Physical Layer (PHY) Specifications for," *IEEE Std 802.15.4-2003*, pp. 0_1–670, 2003.

[16] J. A. Stankovic, "Research Directions for the Internet of Things," *Internet of Things Journal, IEEE*, vol. 1, no. 1, pp. 3–9, 2014.

[17] N. Majedi, M. Naeem, and A. Anpalagan, "Telecommunication integration in e-healthcare: technologies, applications and challenges," *Transactions on Emerging Telecommunications Technologies*, vol. 25, no. 3, pp. n/a–n/a, 2016.

[18] FDA CDRH, "Guidance Documents (Medical Devices and Radiation-Emitting Products) - Radio Frequency Wireless Technology in Medical Devices - Guidance for Industry and Food and Drug Administration Staff," 2013. [Online]. Available: http://www.fda.gov/MedicalDevices/DeviceRegulationandGuidance/GuidanceDocuments/ucm077210.htm

[19] V. Cellini and G. Dona, "A Novel Joint Channel and Multi-User Interference Statistics Estimator for UWB-IR based on Gaussian Mixture Model," in *2005 IEEE International Conference on Ultra-Wideband*, no. 1. IEEE, 2005, pp. 655–660.

[20] Y. Sheng, K. Tan, G. Chen, D. Kotz, and A. Campbell, "Detecting 802.11 MAC layer spoofing using received signal strength," *Proceedings - IEEE INFOCOM*, pp. 2441–2449, 2008.

[21] N. Gulati, R. Greenstadt, K. R. Dandekar, and J. M. Walsh, "GMM based semi-supervised learning for channel-based authentication scheme," *IEEE Vehicular Technology Conference*, 2013.

[22] W. Wang, H. Wang, and M. Hempel, "Secure Stochastic ECG Signals Based on Gaussian Mixture Model for-Healthcare Systems," *Systems Journal, ...*, vol. 5, no. 4, pp. 564–573, 2011.

[23] Y. Zhang, L. Bao, M. Welling, and S. H. Yang, "Base station localization in search of empty spectrum spaces in cognitive radio networks," *MSN 2009 - 5th International Conference on Mobile Ad-hoc and Sensor Networks*, pp. 94–101, 2009.

[24] N. A. Dieng, M. Charbit, C. Chaudet, L. Toutain, and T. Ben Meriem, "Indoor Localization in Wireless Networks Based on a Two-Modes Gaussian Mixture Model," in *2013 IEEE 78th Vehicular Technology Conference (VTC Fall)*. IEEE, sep 2013, pp. 1–5.

[25] M. Alfakih, M. Keche, and H. Benoudnine, "Gaussian mixture modeling for indoor positioning WIFI systems," in *2015 3rd International Conference on Control, Engineering & Information Technology (CEIT)*, no. 1. IEEE, may 2015, pp. 1–5.

[26] C.-H. Min, N. F. Ince, and A. H. Tewfik, "Classification of continuously executed early morning activities using wearable wireless sensors." *Conference proceedings : ... Annual International Conference of the IEEE Engineering in Medicine and Biology Society. IEEE Engineering in Medicine and Biology Society. Conference*, vol. 2008, pp. 5192–5195, 2008.

[27] A. Ahmadi, E. Mitchell, C. Richter, F. Destelle, M. Gowing, N. E. O'Connor, and K. Moran, "Toward automatic activity classification and movement assessment during a sports training session," *IEEE Internet of Things Journal*, vol. 2, no. 1, pp. 23–32, 2015.

[28] T. Q. Le, C. Cheng, A. Sangasoongsong, and S. T. S. Bukkapatnam, "Prediction of sleep apnea episodes from a wireless wearable multisensor suite," *IEEE EMBS Special Topic Conference on Point-of-Care (POC) Healthcare Technologies: Synergy Towards Better Global Healthcare, PHT 2013*, pp. 152–155, 2013.

[29] H. Jiang, S. Chen, Y. Yang, Z. Jie, H. Leung, J. Xu, and L. Wang, "Estimation of Packet Loss Rate at Wireless Link of VANET–RPLE," in *2010 International Conference on Computational Intelligence and Software Engineering*, no. m. IEEE, sep 2010, pp. 1–5.

[30] S. Memon, M. Lech, and N. Maddage, "Speaker Verification Based on Different Vector Quantization Techniques with Gaussian Mixture Models," in *2009 Third International Conference on Network and System Security*. IEEE, 2009, pp. 403–408.

[31] Wade Shen and D. Reynolds, "Improved GMM-based language recognition using constrained MLLR transforms," in *2008 IEEE International Conference on Acoustics, Speech and Signal Processing*. IEEE, mar 2008, pp. 4149–4152.

[32] T. Wang, M. Han, and H. Wan, "Improved and robust eyelash and eyelid location method," *2012 International Conference on Wireless Communications and Signal Processing, WCSP 2012*, 2012.

[33] L. L. Bello and E. Toscano, "Coexistence issues of multiple Co-Located IEEE 802.15.4/ZigBee Networks running on adjacent radio channels in industrial environments," *IEEE Transactions on Industrial Informatics*, vol. 5, no. 2, pp. 157–167, 2009.

[34] F. Lin, C. Chen, N. Zhang, X. Guan, and X. Shen, "Autonomous Channel Switching: Towards Efficient Spectrum Sharing for Industrial Wireless Sensor Networks," *IEEE Internet of Things Journal*, vol. 3, no. 2, pp. 231–243, 2016.

[35] A. P. Dempster, D. B. Rubin, and N. M. Laird, "Maximum Likelihood from Incomplete Data via the EM Algorithm," *Journal of the Royal Statistical Society*, vol. 39, no. 1, pp. 1–38, 1977.

[36] N. Kostantinos, "Gaussian Mixtures and Their Applications to Signal Processing," *Advanced signal processing handbook: theory and implementation for radar, sonar, and medical imaging real time systems*, 2000.

[37] K. Murphy, *Machine Learning: a Probabilistic Perspective*, 2012.

[38] W. Balid, M. O. Al Kalaa, S. Rajab, H. Tafish, and H. H. Refai, "Development of measurement techniques and tools for coexistence testing of wireless medical devices," in *2016 IEEE Wireless Communications and Networking Conference Workshops (WCNCW)*. IEEE, apr 2016, pp. 449–454.

[39] C. Buratti, A. Stajkic, G. Gardasevic, S. Milardo, M. D. Abrignani, S. Mijovic, G. Morabito, and R. Verdone, "Testing protocols for the internet of things on the EuWIn platform," *IEEE Internet of Things Journal*, vol. 3, no. 1, pp. 124–133, 2016.

[40] L. Catarinucci, D. De Donno, L. Mainetti, L. Palano, L. Patrono, M. L. Stefanizzi, and L. Tarricone, "An IoT-Aware Architecture for Smart Healthcare Systems," *IEEE Internet of Things Journal*, vol. 2, no. 6, pp. 515–526, 2015.

[41] International Telecommunication Union (ITU) Radio Sector, "Radio Regulations Article 1 - Terms and Definitions, 1.15," 2012.

[42] "Code of Federal Regulations Title 21, Chapter I, Subchapter H Medical Devices." [Online]. Available: http://www.accessdata.fda.gov/scripts/cdrh/cfdocs/cfCFR/CFRSearch.cfm?FR=860.7

[43] M. Eslami and H. I. Bassen, "A Compact Test System for Simulating Multipath Interference," *Open Journal of Antennas and Propagation*, vol. 02, no. 02, pp. 9–20, 2014.

[44] A. A. Glazunov, V.-M. Kolmonen, and T. Laitinen, "MIMO Over-The-Air Testing," in *LTE-Advanced and Next Generation Wireless Networks*. Chichester, UK: John Wiley & Sons, Ltd, oct 2012, pp. 411–441.

[45] R. Serra and M. Nabi, "Wireless coexistence and interference test method for low-power wireless sensor networks," *IET Science, Measurement & Technology*, vol. 9, no. 5, pp. 563–569, 2015.

[46] A. Sikora and V. Groza, "Coexistence of IEEE802.15.4 with other Systems in the 2.4 GHz-ISM-Band," *2005 IEEE Instrumentationand Measurement Technology Conference Proceedings*, vol. 3, no. May, pp. 1786–1791, 2005.

[47] International Electrotechnical Committee IEC/TC 62/SC 62A, "IEC 60601-1-2:2014: Medical Electrical Equipment – Part 1-2: General Requirements for Basic Safety and Essential Performance – Collateral Standard: Electromagnetic Disturbances – Requirements and Tests," 2014.

[48] R. G. Garroppo, L. Gazzarrini, S. Giordano, and L. Tavanti, "Experimental assessment of the coexistence of Wi-Fi, ZigBee, and Bluetooth devices," in *2011 IEEE International Symposium on a World of Wireless, Mobile and Multimedia Networks*. IEEE, jun 2011, pp. 1–9.

[49] FDA Bureau of Medical Devices, *Electromagnetic compatibility standard for medical devices*. Silver Spring, MD: MDS-201-0004, 1979.

[50] C. A. Hammerschmidt, "NTIA Report TR-14-502, Broadband Spectrum Survey in the Chicago, Illinois, Area," Tech. Rep., 2014.

[51] "Microsoft Spectrum Observatory." [Online]. Available: https://observatory.microsoftspectrum.com/

[52] T. M. Taher, R. B. Bacchus, K. J. Zdunek, and D. a. Roberson, "Long-term spectral occupancy findings in Chicago," *2011 IEEE International Symposium on Dynamic Spectrum Access Networks, DySPAN 2011*, pp. 100–107, 2011.

[53] NTIA, "Spectrum Monitoring Pilot Program Notice of Inquiry," Tech. Rep., 2013.

[54] F. Krug and P. Russer, "The time-domain electromagnetic interference measurement system," *IEEE Transactions on Electromagnetic Compatibility*, vol. 45, no. 2, pp. 330–338, 2003.

[55] G. Noorts, J. Engel, J. Taylor, D. Roberson, R. Bacchus, T. Taher, and K. Zdunek, "An RF spectrum observatory database based on a Hybrid Storage System," *2012 IEEE International Symposium on Dynamic Spectrum Access Networks, DYSPAN 2012*, pp. 114–120, 2012.

[56] M. Hoyhtya, M. Matinmikko, X. Chen, J. Hallio, J. Auranen, R. Ekman, J. Roning, J. Engelberg, J. Kalliovaara, T. Taher, A. Riaz, and D. Roberson, "Measurements and Analysis of Spectrum Occupancy in the 2.3-2.4 GHz band in Finland and Chicago," in *Proceedings of the 9th International Conference on Cognitive Radio Oriented Wireless Networks*. ICST, 2014.

[57] M. Hoyhtya, J. Lehtomaki, J. Kokkoniemi, M. Matinmikko, and A. Mammela, "Measurements and analysis of spectrum occupancy with several bandwidths," in *2013 IEEE International Conference on Communications (ICC)*. IEEE, jun 2013, pp. 4682–4686.

[58] J. Kokkoniemi and J. Lehtomaeki, "Spectrum Occupancy Measurements and Analysis Methods on the 2.45 GHz ISM Band," *Proceedings of the 7th International Conference on Cognitive Radio Oriented Wireless Networks*, pp. 285–290, 2012.

[59] L. Stabellini, "Quantifying and Modeling Spectrum Opportunities in a Real Wireless Environment," in *2010 IEEE Wireless Communication and Networking Conference*. IEEE, apr 2010, pp. 1–6.

[60] M. H. Islam, C. L. Koh, S. W. Oh, X. Qing, Y. Y. Lai, C. Wang, Y.-c. Liang, B. E. Toh, F. Chin, G. L. Tan, and W. Toh, "Spectrum Survey in Singapore: Occupancy Measurements and Analyses," in *2008 3rd International Conference on Cognitive Radio Oriented Wireless Networks and Communications (CrownCom 2008)*. IEEE, may 2008, pp. 1–7.

[61] T. Harrold, R. Cepeda, and M. Beach, "Long-term measurements of spectrum occupancy characteristics," *2011 IEEE International Symposium on Dynamic Spectrum Access Networks, DySPAN 2011*, pp. 83–89, 2011.

[62] R. De Francisco and A. Pandharipande, "Spectrum occupancy in the 2.36-2.4 GHz band: Measurements and analysis," *2010 European Wireless Conference, EW 2010*, pp. 231–237, 2010.

[63] M. López-Benítez, "Spectrum usage models for the analysis, design and simulation of cognitive radio networks," Ph.D. dissertation, Universitat Politècnica de Catalunya, 2011.

[64] M. Lopez-Benitez and F. Casadevall, "Methodological aspects of spectrum occupancy evaluation in the context of cognitive radio," in *2009 European Wireless Conference*, no. September. IEEE, may 2009, pp. 199–204.

[65] M. López-Benítez and F. Casadevall, "On the spectrum occupancy perception of cognitive radio terminals in realistic scenarios," *2010 2nd International Workshop on Cognitive Information Processing, CIP2010*, pp. 99–104, 2010.

[66] ——, "Empirical time-dimension model of spectrum use based on a discrete-time Markov chain with deterministic and stochastic duty cycle models," *IEEE Transactions on Vehicular Technology*, vol. 60, no. 6, pp. 2519–2533, 2011.

[67] S. Krishnamoorthy, J. Reed, C. Anderson, P. Max Robert, and S. Srikanteswara, "Characterization of the 2.4 GHz ISM band electromagnetic interference in a hospital environment," in *Proceedings of the 25th Annual International Conference of the IEEE Engineering in Medicine and Biology Society (IEEE Cat. No.03CH37439)*, vol. 4. IEEE, 2003, pp. 3245–3248.

[68] K. Takizawa, A. Aoyagi, J.-I. Takada, N. Katayama, K. Yekeh, Y. Takehiko, and K. R. Kohno, "Channel models for wireless body area networks." *Conference proceedings : ... Annual International Conference of the IEEE Engineering in Medicine and Biology Society. IEEE Engineering in Medicine and Biology Society. Conference*, vol. 2008, pp. 1549–1552, 2008.

[69] O. Lauer, D. Barras, M. Zahner, R. Vahldieck, H. Jackel, and J. Frohlich, "Interference characterization and UWB channel measurements for wireless intensive care patient monitoring," in *2009 International Conference on Electromagnetics in Advanced Applications*, 2009, pp. 613–616.

[70] N. J. LaSorte, W. J. Barnes, and H. H. Refai, "Characterization of the electromagnetic environment in a hospital and propagation study," in *2009 IEEE International Symposium on Electromagnetic Compatibility*. IEEE, aug 2009, pp. 135–140.

[71] M. Uno, T. Miyasaka, K. Yano, and M. Ariyoshi, "A Proposal of QoE Based Self-Organized Wireless System Considering the Measurement Results in a Major Hospital," in *Modeling & Optimization in Mobile, Ad Hoc & Wireless Networks (WiOpt), 2013 11th International Symposium on*, Tsukuba Science City, 2013, pp. 101 – 106.

[72] M. Virk, R. Vuohtoniemi, M. Hämäläinen, J.-P. Mäkelä, and J. Iinatti, "Spectrum Occupancy Evaluations at 2.35-2.50 GHz ISM Band in a Hospital Environment," in *Proceedings of the 9th International Conference on Body Area Networks*, vol. 6, 2014.

[73] M. H. Virk, R. Vuohtoniemi, M. Hamalainen, J. Iinatti, and J.-P. Makela, "Stochastic spectral occupancy modeling: A body area network perspective in ISM band," in *2015 9th International Symposium on Medical Information and Communication Technology (ISMICT)*. Kamakura, Japan: IEEE, mar 2015, pp. 157–161.

[74] L. Mucchi, A. Carpini, T. D'Anna, M. H. Virk, R. Vuohtoniemi, M. Hamalainen, and J. Iinatti, "Threshold setting for the evaluation of the aggregate interference in ISM band in hospital environments," in *2015 9th International Symposium on Medical Information and Communication Technology (ISMICT)*, 2015, pp. 20–24.

[75] L. Mucchi and A. Carpini, "Aggregate Interference in ISM Band: WBANs need cognitivity?" in *Proceedings of the 9th International Conference on Cognitive Radio Oriented Wireless Networks*. ICST, 2014, pp. 1–7.

[76] M. O. A. Kalaa, W. Balid, N. Bitar, and H. H. Refai, "Evaluating Bluetooth Low Energy in realistic wireless environments," in *2016 IEEE Wireless Communications and Networking Conference*. IEEE, apr 2016, pp. 1–6.

[77] "IEEE Recommended Practice for Information technology– Local and metropolitan area networks– Specific requirements– Part 15.2: Coexistence of Wireless Personal Area Networks with Other Wireless Devices Operating in Unlicensed Frequency Bands," pp. 1–150, 2003.

[78] F. Huang, Z. Jiang, S. Zhang, and S. Gao, "Reliability Evaluation of Wireless Sensor Networks Using Logistic Regression," *2010 International Conference on Communications and Mobile Computing*, pp. 334–338, 2010.

[79] T. Liu, S. Wang, S. Wu, J. Ma, and Y. Lu, "Predication of wireless communication failure in grid metering automation system based on logistic regression model," in *2014 China International Conference on Electricity Distribution (CICED)*, Intergovernmental Panel on Climate Change, Ed., vol. 53, no. 9. Cambridge: IEEE, sep 2014, pp. 894–897.

[80] R. R. Tanuhardja, L. A. Gonzalez, C. M. Wang, W. F. Young, K. A. Remley, and J. M. Ladbury, "Using the amplitude variation of a reverberation chamber channel to predict the synchronization of a wireless digital communication test system," *IEEE International Symposium on Electromagnetic Compatibility*, vol. 2015-Septm, pp. 171–176, 2015.

[81] T. Liu and A. E. Cerpa, "Foresee (4C): Wireless link prediction using link features," *Proceedings of the 10th ACM/IEEE International Conference on Information Processing in Sensor Networks*, pp. 294–305, 2011.

[82] S. Srivastava, M. Hashmi, S. Das, and D. Barua, "Real-time blind spectrum sensing using USRP," *Proceedings - IEEE International Symposium on Circuits and Systems*, vol. 2015-July, pp. 986–989, 2015.

[83] M. I. Tiwana, B. Sayrac, Z. Altman, and T. Chahed, "Statistical learning-based automated healing: Application to mobility in 3g LTE networks," *IEEE International Symposium on Personal, Indoor and Mobile Radio Communications, PIMRC*, pp. 1746–1751, 2010.

[84] A. Thampi, S. Armour, and D. Kaleshi, "A logistic regression approach to location classification in OFDMA-based FFR systems," *2013 IEEE 14th International Symposium on "A World of Wireless, Mobile and Multimedia Networks" (WoWMoM)*, pp. 1–9, 2013.

[85] Y. Qiang, X. Chang, J. Zhao, X. Zhang, and X. Yan, "A New Energy Reduction Method Based on Fire Probability Threshold Switch for WSN," *2014 10th International Conference on Mobile Ad-hoc and Sensor Networks*, pp. 30–37, 2014.

[86] G. Boverman and S. Genc, "Prediction of mortality from respiratory distress among long-term mechanically ventilated patients," *Conference proceedings : ... Annual International Conference of the IEEE Engineering in Medicine and Biology Society. IEEE Engineering in Medicine and Biology Society. Annual Conference*, vol. 2014, pp. 3464–3467, 2014.

[87] M. Etemadi, S. Hersek, J. M. Tseng, N. Rabbani, J. A. Heller, S. Roy, L. Klein, and O. T. Inan, "Tracking clinical status for heart failure patients using ballistocardiography and electrocardiography signal features," *2014 36th Annual International Conference of the IEEE Engineering in Medicine and Biology Society, EMBC 2014*, vol. 94143, pp. 5188–5191, 2014.

[88] R. Tibshirani, "Regression Shrinkage and Selection via the Lasso," *Journal of the Royal Statistical Society. Series B (Methodological)*, vol. 58, no. 1, pp. 267–288, 1996.

[89] J. Friedman, T. Hastie, and R. Tibshirani, "Regularization Paths for Generalized Linear Models via Coordinate Descent," *Journal of Statistical Software*, vol. 33, no. 1, pp. 2008–2010, 2010.

[90] N. J. LaSorte, S. A. Rajab, and H. H. Refai, "Experimental assessment of wireless coexistence for 802.15.4 in the presence of 802.11g/n," in *2012 IEEE International Symposium on Electromagnetic Compatibility*. IEEE, aug 2012, pp. 473–479.

[91] G. Wheeler, "The Lasso Logistic Regression Model: Modifications to aid causality assessment for Adverse Events Following Immunization," Ph.D. dissertation, 2010.

[92] J. J. Goeman, "L1 penalized estimation in the Cox proportional hazards model." *Biometrical journal. Biometrische Zeitschrift*, vol. 52, no. 1, pp. 70–84, feb 2010.

[93] J. Riihijarvi, P. Mahonen, M. Wellens, and M. Gordziel, "Characterization and modelling of spectrum for dynamic spectrum access with spatial statistics and random fields," in *2008 IEEE 19th International Symposium on Personal, Indoor and Mobile Radio Communications*. IEEE, sep 2008, pp. 1–6.

[94] International Organization for Standardization (ISO), "ISO 5725-1:1994 Accuracy (trueness and precision) of measurement methods and results — Part 2: Basic method for the determination of repeatability and reproducibility of a standard measurement method," 1994.

Appendices

Chapter A: Repeatability and reproducibility of radiated open environment coexistence testing

A.1. Introduction

In this appendix, the repeatability and reproducibility of line-of-sight (LOS) radiated open environment coexistence testing (ROECT) is investigated and quantified. The studied testing layout is illustrated in Figure 4.1. The standard ISO 5725-1,2:1994—Part 2 regulates the determination of repeatability and reproducibility of a standard measurement method [94]. Repeatability value quantifies the deviation of coexistence testing results under repeatability conditions (i.e., same method, identical test items, same laboratory, same operator, same equipment, within short intervals of time). Reproducibility value quantifies the deviation of coexistence testing results when performed in distinct environments or in laboratories under reproducibility conditions (i.e., same method, identical test items, different laboratories, different operators, same equipment).

We draw an analogy between the laboratories referred to in ISO 5725-1,2 and the realistic wireless environments wherein ROECT could be conducted. Consequently, ROECT is evaluated under repeatability and reproducibility conditions to derive

the standard deviation values thereof. The considered system-under-test (UTS) is a ZigBee system wherein the packet error rate (PER) is used as a key performance indicator (KPI). Wi-Fi (IEEE 802.11g and IEEE 802.11n) was investigated as the interfering systems (IS).

Propagation phenomena in distinct indoor environments could affect the received power level at UTS receiver antenna. Consequently, demodulation of received signal and ROECT testing outcome could vary when repeated in other laboratories. To limit these effects when repeating ROECT, a condition is added to the testing procedure with the UTS transmitter and receiver observe signal levels as close as possible to those in the reference laboratory.

Following in Section A.2, mathematical formulation of repeatability and reproducibility is introduced. Section A.3 elaborates on the implemented ROECT testing procedure. Experimental results are presented in Section A.4, and Section A.5 concludes the appendix.

A.2. Mathematical formulation

A.2.1 Repeatability

The arithmetic mean of the within-laboratory variance taken over all laboratories taking part in the experiment is used as an estimate of the repeatability variance.

$$s_{rj}^2 = \frac{\sum_{i=1}^{p}(n_{ij}-1)s_{ij}^2}{\sum_{i=1}^{p}(n_{ij}-1)} \tag{A.1}$$

where j is a reference to the measured level (i.e., PER at a given IS throughput); i is a reference to one of the test replicates in one of the involved laboratories (i.e., environments); p is the count of involved laboratories; s_{ij} is the standard deviation of repetitions in i^{th} set of measurement for level j; and n_{ij} is the count of repetitions in i^{th} set of measurement for level j.

A.2.2 Reproducibility

The summation of the repeatability variance and the between-laboratory variance is used as an estimate of the reproducibility variance, which reflects maximum variability in results.

$$s_{Rj}^2 = s_{rj}^2 + s_{Lj}^2 \tag{A.2}$$

where s_{Lj}^2 is the estimate of the between-laboratory variance.

$$s_{Lj}^2 = \frac{s_{dj}^2 - s_{rj}^2}{\bar{\bar{n}}_j} \tag{A.3}$$

$$s_{dj}^2 = \frac{1}{p-1}\left[\sum_{i=1}^{p} n_{ij}\left(\bar{y}_{ij}\right)^2 - \left(\bar{\bar{y}}_j\right)^2 \sum_{i=1}^{p} n_{ij}\right] \tag{A.4}$$

$\bar{\bar{y}}_j$ is the grand mean of test results.

$$\bar{\bar{y}}_j = \frac{\sum_{i=1}^{p} n_{ij}\bar{y}_{ij}}{\sum_{i=1}^{p} n_{ij}} \tag{A.5}$$

$\bar{y}_{ij}$ is the mean of results in i^{th} set of measurement for level j.

$$\bar{y}_{ij} = \frac{1}{n_{ij}} \sum_{k=1}^{n_{ij}} y_{ijk} \tag{A.6}$$

$$\bar{\bar{n}_j} = \frac{1}{p-1} \left[\sum_{i=1}^{p} n_{ij} - \frac{\sum_{i=1}^{p} n_{ij}^2}{\sum_{i=1}^{p} n_{ij}} \right] \tag{A.7}$$

A.3. Procedure

LOS ROECT experimental layout is depicted in Figure 4.1. A reference setup is deployed in an anechoic chamber operated by the Wireless Electromagnetic Compliance and Design Center (WECAD) at the University of Oklahoma-Tulsa. When repeating the experiment, care was taken to instal IS and UTS nodes (i.e., spatial distribution or transmission power of IS and UTS if nodes permit control) to maintain identical received power levels at the UTS receiver antenna. Specifically, UTS received signal strength (RSS) and observed IS power level at UTS nodes locations are preserved.

The following enumerates testing procedure:

1. Measure noise floor.
2. Ensure negligible PER with baseline UTS communication.
3. Commence IS at a given constant throughput.
4. Commence UTS communication in the presence of interference.
5. Measure and log:
   (a) RSSI for UTS.

(b) Average IS power at UTS transmitter $P_{av,Tx}$.

(c) Peak IS power at UTS transmitter $P_{pk,Tx}$.

(d) Average IS power at UTS receiver $P_{av,Rx}$.

(e) Peak IS power at UTS receiver $P_{pk,Rx}$.

6. Log PER reading from UTS.

Steps 3-6 are performed for all channel utilization cases of interest.

A ZigBee system comprising one transmitter node and one receiver node is used as UTS. During testing for a given IS network throughput, UTS Tx sends 1000 packets to UTS Rx, and PER is calculated as the ratio of correctly received packets to total number of transmitted packets.

A.4. Results

A.4.1 IS is 802.11n

Two environments were included: 1) anechoic chamber and 2) laboratory room. The laboratory room is located in a semi-underground establishment. UTS PER was measured for 11 levels of IS throughput. Each test run was repeated five times.

Results are presented in Figure A.1. UTS PER as a function of IS throughput is plotted in Figure A.1(a) where error bars represent mean of calculated PER at the center and bar length is twice the PER standard deviation. PER results in lab room environment are shown to match those obtained in the anechoic chamber. In addition to IS CU, the same can be observed for the various monitored power levels during

testing. See Figure A.2. Standard deviations of repeatability and reproducibility are presented in Figure A.1(b). Average repeatability was 1.16%, and average reproducibility was 1.62%.

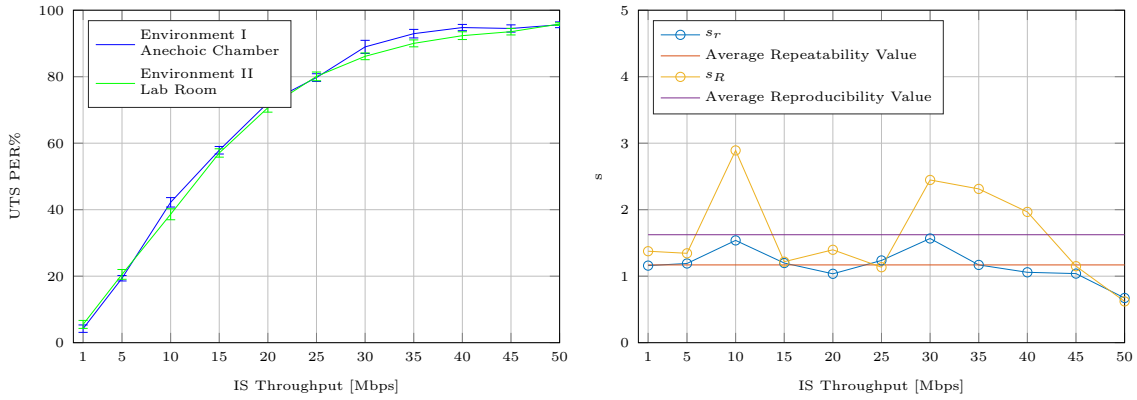

(a) UTS PER **(b)** Repeatability and Reproducibility

Figure A.1. UTS PER and Repeatability and Reproducibility for ROECT when IS was 802.11n

A.4.2 IS is 802.11g

Identical environments (i.e., anechoic chamber as reference and laboratory room) were used when IS was operating 802.11g. UTS PER was measured for 15 levels of IS throughput. Each test run was repeated five times. Results are presented in Figure A.3. UTS PER as a function of IS throughput is plotted on Figure A.3(a). Matching trends for UTS PER and other monitored variables are verified (See Figure A.4). Standard deviations of repeatability and reproducibility are presented in Figure A.1(b). Average repeatability was 1.35%, and average reproducibility was 1.55%.

A third environment was evaluated to represent an extreme case of indoor environments with numerous metal reflectors on the ceiling. This room, denoted as "lab with reflectors," was located in the same lab room building as used previously in the

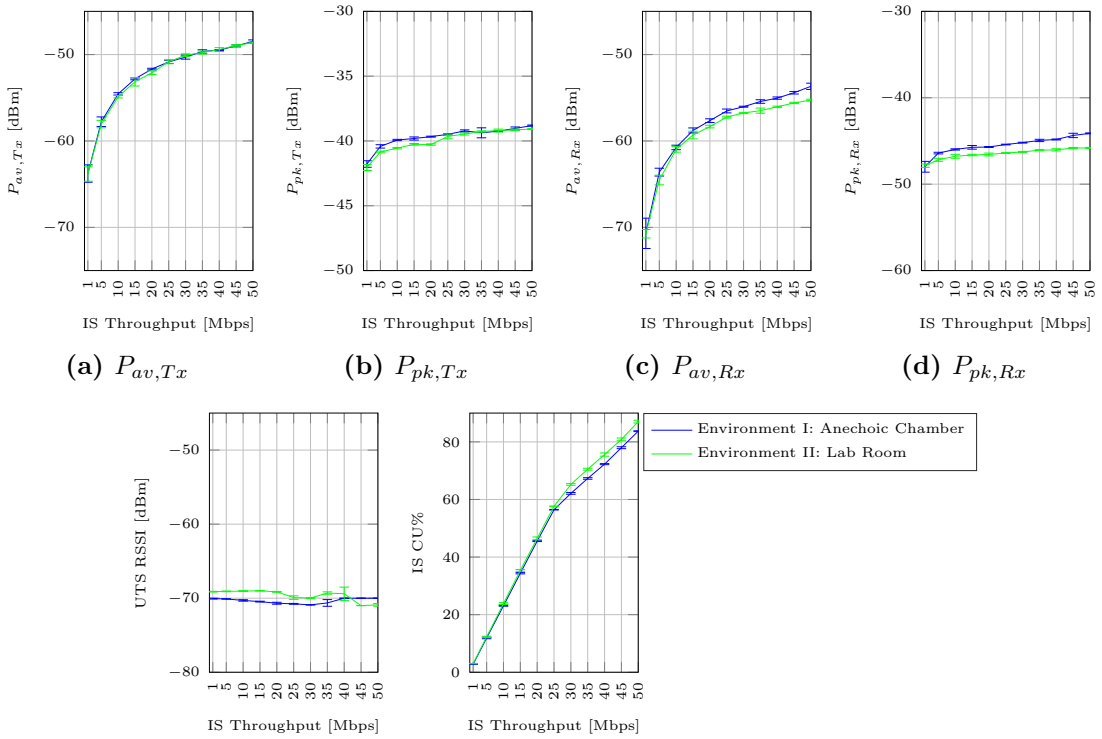

(a) $P_{av,Tx}$ **(b)** $P_{pk,Tx}$ **(c)** $P_{av,Rx}$ **(d)** $P_{pk,Rx}$

(e) UTS RSSI **(f)** IS CU

Figure A.2. Monitored variables during ROECT when IS was 802.11n

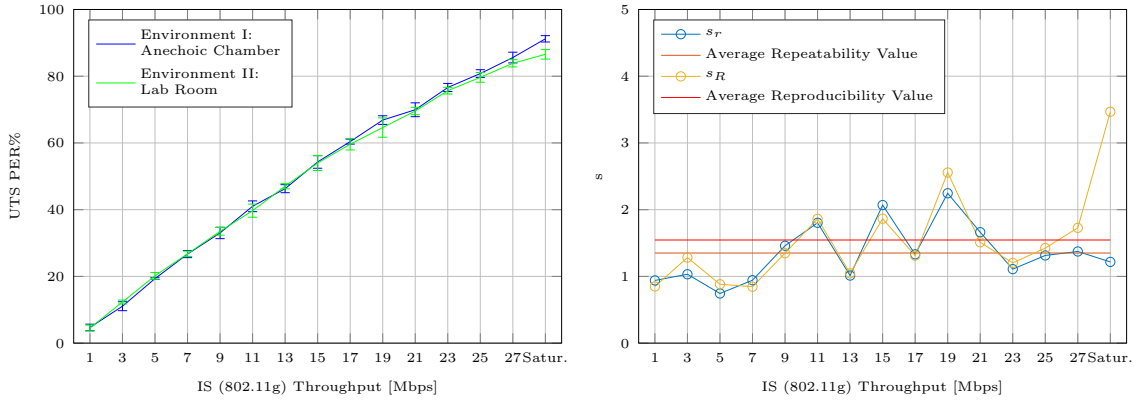

(a) UTS PER **(b)** Repeatability and Reproducibility

Figure A.3. UTS PER and Repeatability and Reproducibility for ROECT when IS was 802.11g evaluated in two environments

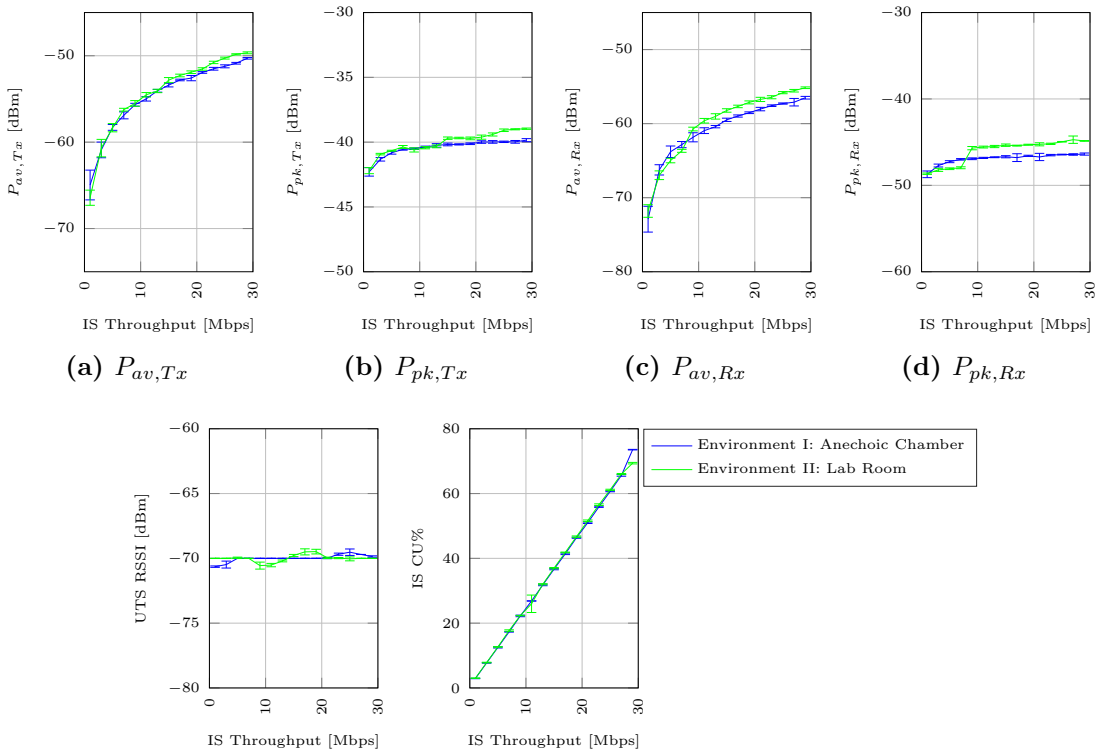

(a) $P_{av,Tx}$ **(b)** $P_{pk,Tx}$ **(c)** $P_{av,Rx}$ **(d)** $P_{pk,Rx}$

(e) UTS RSSI **(f)** IS CU

Figure A.4. Monitored variables during ROECT when IS was 802.11g evaluated in two environments

study. Having metal reflectors in this environment increases the chance of adding reflected signals either constructively or destructively following their phases at the UTS Rx antenna. Consequently, increased randomness can be expected as a measurement outcome.

The experiment was repeated in the lab with reflectors, and results were incorporated in repeatability and reproducibility calculations. UTS PER followed the same trend observed in the anechoic chamber and the lab room, as seen in Figure A.5(a). Notably, UTS PER had higher values in the lab with reflectors. This increase in UTS PER values contributed to the increase in reproducibility standard deviation illustrated in Figure A.5(b). When considering UTS PER measurement outcomes of

the three environments, average repeatability was 1.25% and average reproducibility was 4.19%.

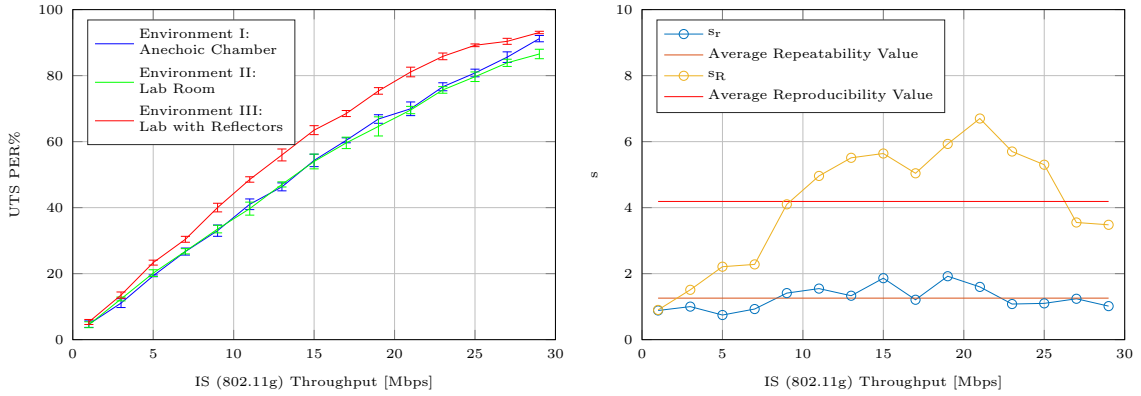

(a) UTS PER **(b)** Repeatability and Reproducibility

Figure A.5. UTS PER and Repeatability and Reproducibility for ROECT when IS was 802.11g evaluated in three environments

A.5. Conclusion

An evaluation of repeatability and reproducibility of LOS ROECT was presented in this appendix. Following ROECT procedure, focused attention ensured that observed IS and UTS power levels at UTS Rx node were maintained under both repeatability and reproducibility conditions. An RF anechoic chamber was used as a reference environment, and a laboratory room was used to repeat the experimental work. Average repeatability was 1.16% and 1.35% when IS was 802.11n and 802.11g, respectively. Reproducibility was 1.62% and 1.55% when IS was 802.11n and 802.11g, respectively. When a third environment with metal reflective surfaces on the ceiling was included in the study and IS was 802.11g, repeatability was 1.25% and reproducibility was 4.19%.

Acknowledgment

Thanks go to Samer Rajab for establishing the idea that maintaining constant power levels at involved nodes would enhance the repeatability and reproducibility of testing. Bashar Romanous and Fahd Babelli are acknowledged for their participation in performing the test runs that generated the evaluated dataset.